UNIVERSITY OF CALIFORNIA
RIVERSIDE

Oxidation Kinetics of Pyrite in Synthetic Seawater: Implications for Seafloor Mining Operations

A Thesis submitted in partial satisfaction
of the requirements for the degree of

Master of Science

in

Geological Sciences

by

Taylor Alexander van Hoorebeke

December 2016

Thesis Committee:

Dr. Michael A. McKibben, Chairperson
Dr. Gordon Love
Dr. Andrey Bekker

The Thesis of Taylor Alexander van Hoorebeke is approved:

_____

_____

_____
Committee Chairperson

University of California, Riverside

Acknowledgments

Considerable credit must be given to my graduate thesis advisor, Dr. Michael McKibben. In addition to conceiving the idea for this project, Dr. McKibben received an NSF research grant that funded the research and provided me with a salary as a graduate student researcher. I am especially grateful for the opportunity to work in the geochemical kinetics lab and to have gained so much practical experience in a wet-chemistry lab. Mike - Thank you again for your sound advice and constant encouragement over the past two years, it was a pleasure serving as your final graduate student.

A great deal of gratitude is extended towards my laboratory assistant Natalie Alsalek. Despite being initially hired for only the summer 2014 term, Natalie was consistently determined to continue working in the geochemical kinetics lab throughout my time as a graduate student. Natalie's kind advice and light-hearted humor always made her a pleasure to spend those extended experiment hours with. Natalie - thank you for always putting in the extra effort, and for going above and beyond both Mike's and my expectations.

Special thanks to Andy Robinson, the resident ICP-MS expert, for his patience and commitment towards excellence in sample analysis. Andy - Thank you for frequently donating time beyond your pay allowance to help me analyze samples in a time efficient manner. Additional thanks to Steve Bates for his suggestions for improving general lab practices, including his advice on reducing chemical noise in analytes. Finally, thank you to Dr. Tim Lyons for use of the ICP-MS in his laboratory.

Dedication

This thesis is dedicated to my mother Melodee van Hoorebeke. Thank you for always believing in me and for consistently encouraging me to pursue the career of my choice. You are the backbone of support I can always count on, and for that I am eternally grateful. I love you mom!

ABSTRACT OF THE THESIS

Oxidation Kinetics of Pyrite in Synthetic Seawater: Implications for Seafloor Mining Operations

by

Taylor Alexander van Hoorebeke

Master of Science, Graduate Program in Geological Sciences
University of California, Riverside, December 2016
Dr. Michael A. McKibben, Chairperson

As the demand for industrial materials rises, mining companies have become increasingly interested in exploiting unconventional metal resources. Seafloor massive sulfide (SMS) deposits, one such example of an unconventional resource, will be mined for their high ore grade and abundance along oceanic plate margins. As these deposits are mined, fresh and highly reactive surfaces of sulfide minerals will be exposed to seawater, causing them to immediately oxidize. Pyrite (FeS_2) is

the most common sulfide mineral and readily oxidizes under atmospheric conditions. Sulfuric acid is a product of the sulfide mineral oxidation process and is often responsible for the devastating effects of acid mine drainage at terrestrial mining sites.

Kinetics experiments have been conducted to determine a rate law for the abiotic rate of pyrite oxidation in synthetic seawater. Experiments run from pH 2-5, 0.995 or 0.10 atm O_2, and temperatures of 285 – 303 K were used in rate law calculations. The experimentally derived molal specific rate law is:

$$R_{sp} = -10^{-11.02\pm0.03}[H^+]^{0.39\pm0.03}[P_{O2}]^{0.44\pm0.05}$$

where $[H^+]$ and $[P_{O2}]$ represent the initial molal concentrations of protons and dissolved oxygen in the seawater, and the rate R_{sp} is in units of moles m^{-2} sec^{-1}. The initial rate method was combined with the method of isolation to determine the effects that pH, dissolved oxygen concentration, and temperature have on the pyrite oxidation rate. Results show that the initial concentration of dissolved oxygen is more influential upon the initial pyrite oxidation rate than the initial pH of the seawater under acidic, low temperature conditions.

The pyrite oxidation rate in acidic seawater is the slowest of the sulfides pyrite, pyrrhotite, and chalcopyrite, with the reaction proceeding up to three orders of magnitude slower than that of pyrrhotite in synthetic seawater. The slow pyrite weathering rate (whether natural or anthropogenically induced) enhanced pyrite preservation in massive sulfide deposits. This may explain why VMS deposits are more enriched in pyrite than any other sulfide mineral.

Table of Contents

List of Figures

List of Tables

Introduction

Pyrite and Acid Mine Drainage

Pyrite (FeS_2) is the most abundant sulfide mineral in the Earth's crust. It is found in a wide variety of rocks and geological formations.

The oxidation kinetics of pyrite has been studied extensively (Garrels and Thompson, 1960; Singer and Stumm, 1970; Nordstrom, 1982; McKibben, 1984; McKibben and Barnes, 1986; Rimstidt and Vaughan, 2003; and many others). The oxidation of pyrite is an irreversible reaction that can be affected by water, dissolved oxygen or ferric iron, and catalyzed by certain strains of bacteria. As with other sulfide minerals, the oxidation of pyrite occurs naturally as the mineral is subjected to the oxidizing conditions of the atmosphere (Singer and Stumm, 1970). Reactions for pyrite oxidation via 1. dissolved oxygen and 2. ferric iron are:

Equation 1. $FeS_2 + 3.5O_2 + H_2O = Fe^{2+} + 2SO_4^{2-} + 2H^+$

Equation 2. $FeS_2 + 14Fe^{3+} + 8H_2O = 15Fe^{2+} + 2SO_4^{2-} + 16H^+$

Sulfuric acid is a product of the sulfide mineral oxidation process and is also one of the main sources of a type of terrestrial pollution known as acid mine drainage (AMD). Because groundwater and most surface waters have low buffer capacities they are not capable of neutralizing localized spikes in acidity caused by sulfide mineral oxidation. The devastating effects of AMD in freshwater are well documented (Nordstrom and Alpers, 1999; Figures 1, 2).

Pyrite is associated with most types of metallic ore deposits even though it is not an economic mineral. This leads to a significant environmental issue: common base metal mines (as well as coal mines) produce large amounts of pyrite in ore but the pyrite is not of economic or industrial value. Mine operators often leave pyrite and other gangue minerals in waste piles, called tailings, adjacent to the mine. Sulfuric acid generated from the natural weathering of pyrite-rich mine tailings is arguably the most well known source of AMD in the United States.

It is important to follow the market trends of mineral commodities because the extent that a resource is exploited is largely controlled by the market value of that resource. In December 2015 metal commodities such as copper and zinc had fallen to their lowest values since the global financial crisis of 2009 (Figure 3). Commodity prices were primarily overwhelmed by excessive supply and soft demand, particularly from struggling national economies such as Brazil and China (IMF Report, Jan. 2016).

Late into August 2016 the worldwide mineral market continued to struggle. Decreased demand for steel and a drop in oil prices were largely responsible for reduced market activity, despite efforts by China and other countries to introduce policies to protect the construction industry (IMF Report, July 2016). The International Monetary Fund (IMF) stated that expected slow growth in strong economies, and uncertainty tied to the United Kingdom Referendum, limited projected market improvements for the remainder of the calendar year (IMF Report, July 2016). This would expectedly translate to fewer new mineral projects being

developed and drastic cost-shaving practices being undertaken at existing operations.

The value of a commodity may be indicative of the level of innovation that a particular sector will experience. With the eventual recovery of the mineral market there will come a need to meet high demand. As the value of metals rises again, commercially unconventional mineral resources may become the new targets of mining companies.

Seafloor Massive Sulfide Deposits

Seafloor massive sulfide (SMS) deposits are examples of currently unconventional metal resources that may become mining prospects once the base metal commodity market recovers. SMS deposits are a type of hydrothermal ore deposit that forms on the seafloor. They are the modern analogue of ancient volcanogenic massive sulfide (VMS) deposits, which are terrestrial sulfide deposits of relatively high ore grade. SMS deposits typically form near oceanic spreading centers, but they may also be found in back-arc basins and submarine volcanic arc chains associated with convergent margins (Figure 4). SMS deposits were originally discovered from strong electromagnetic anomalies detected on the seafloor (Tivey, 2007).

Figure 5 depicts a common process by which seafloor massive sulfide deposits can form (Herzig *et al.*, 2000). The uppermost 0.5-1 km of oceanic crust is characterized by the presence of basalt, an aphanitic igneous rock enriched in mafic

minerals, overlain by unconsolidated marine sediment. A buried magma chamber heats seawater that percolates into fractured basaltic crust. As it is heated, this seawater is reduced by interaction with the basalt and transformed into a hot hydrothermal fluid capable of leaching metals from the surrounding basaltic host rock. The hydrothermal fluid may interact with magmatic fluids rising from the magma chamber. When this hot (up to 400°C) fluid carrying dissolved metals and reduced sulfur is exhaled into cold seawater (as low as 2°C at 1500m depth), sulfide minerals immediately precipitate out and form accumulates on the seafloor. Figure 6 shows an example of an active submarine fumarole, a type of hydrothermal vent.

Massive sulfide deposits are attractive mining prospects even though they lie at the bottom of the ocean. SMS deposits contain higher concentrations of ore relative to terrestrial sulfide deposits (Hoagland *et al.*, 2010). Recently discovered massive sulfide bodies are on average ten times more enriched in ore than world-class porphyry deposits (Herzig *et al.*, 2000; Tivey, 2007). SMS deposits can also be exploited with minimally invasive mining techniques, in stark contrast to open pit mining procedures used at porphyry and VMS sites. SMS deposits are laterally extensive ore deposits with a centralized mound of massive sulfide where exhalation of the metal-rich fluid originated. Since these deposits form with little or no overburden they can be mined with tractor-like mining tools that grind the surface of the seafloor (Nautilus, 2014).

As of July 2016 two mining companies have publicly expressed interest in exploiting seafloor massive sulfide deposits. Canada-based Nautilus Minerals and

Neptune Minerals of Florida have each developed detailed plans by which they plan to mine seafloor sulfide deposits. The first projected seafloor mining site, called Solwara 1, is located in the Bismarck Sea near Papua New Guinea at a depth of 1600 meters. A 20-year mining lease for production of the Solwara 1 site was granted to Nautilus by the government of Papua New Guinea in 2011. This was the first deep sea mining lease ever granted.

Figure 7 helps to visualize the ore recovery process that was proposed by Nautilus Minerals in 2014. There are five components to this ore recovery process and they include the *in situ* pulverization of sulfide mounds on the seafloor, collection and transport of the crushed sulfide to the ship via the riser and lifting system, separation of ore from waste material on the ship surface, and the return of the waste slurry to the deep ocean. Nautilus' proposed ore recovery process allows several distinct opportunities for pyrite oxidation in addition to that occurring during pulverization on the seafloor. These locations mark zones where the conditions for oxidation are optimized.

Thermodynamics predicts that the likelihood of pyrite oxidation will increase in the warmer, more oxygenated surface waters of the ocean and on the surface of the ore-processing ship. ΔG^0, the standard-state Gibbs free energy of a system, can be used to predict the level of spontaneity of a particular reaction via the following equation:

Equation 3. $\Delta G^0 = -\mathrm{RT} \ln K$

where R is the gas constant (8.314 kJ mol^{-1} K^{-1}), T is the temperature in Kelvin, and K is the equilibrium constant. Figure 8 depicts a table of equilibrium constants calculated by Rxn, a Geochemist's Workbench software program designed to automatically balance chemical reactions (Bethke, 2009). According to Equation 3, ΔG^0 is inversely proportional to the temperature of the system. Since the Gibbs free energy of a system is negative for all spontaneous reactions, increasing the temperature of the system will increase the likelihood that the pyrite oxidation reaction will occur.

The exploitation of SMS deposits will certainly have physical and chemical effects on the local marine environment that have not yet been fully quantified. In September 2008 Nautilus submitted an Environmental Impact Statement (EIS) for the Solwara 1 project to the government of Papua New Guinea that was largely based on the mining practices and environmental impacts of existing terrestrial copper mines (Nautilus 2008). The EIS was compiled by Coffey Natural Systems, an Australian consulting firm, and was commissioned by Nautilus. The EIS was not thorough, as it did not consider all possible scenarios that may adversely affect the environment during SMS mining activities. For example, Nautilus failed to provide details for how they would respond to chemical spillage caused by storms, what the immediate impact anthropogenic sediment plumes will have on marine life and the local fishing industry, and specific levels of metal toxicity for those marine species that are most at risk from mining activities.

The overlying problem with these new mining ventures is the lack of thorough scientific data that investigates their potential consequences. This is an issue that cannot be overlooked because in many respects the deep ocean is uncharted territory.

Van Dover (2011) makes an interesting comparison between today's seafloor and nineteenth century Yellowstone. Before it was established as a national park Yellowstone was a largely unexplored landscape. Today it is easy to see the immense loss that would have occurred had the US government sold miners the land rights to Yellowstone in 1872. It can be argued that much less is known about the deep ocean floor today than explorers knew of Yellowstone 150 years ago. There is still so much to learn and appreciate in the deep ocean. It would be irresponsible to pulverize and mine the seafloor before thorough ecological studies have been conducted.

Previous Studies

Previous sulfide oxidation kinetics studies performed by Bilenker (2011) and Romano (2011) yielded rate laws for chalcopyrite and pyrrhotite oxidation in artificial seawater, respectively. Both researchers found that the rate laws for sulfide oxidation were more dependent upon the initial dissolved oxygen concentration than the initial pH, though the rate dependence on oxygen for chalcopyrite (1.22) was four times greater than that of pyrrhotite (0.30).

Interestingly, both studies concluded that pH did not have much of an effect on the rate when the initial seawater pH measured <4.

Based on their results, the researchers predicted the rate for pyrite oxidation in seawater to fall between the pyrrhotite and chalcopyrite rate laws. This hypothesis seemed logical since the chalcopyrite oxidation rate, as was originally presented by Rimstidt *et al.* (1993), was so low compared to other sulfide minerals.

Reaction Stoichiometry & Rate-Determining Variable

A stoichiometric mass balance for pyrite oxidation based on Equation 1 may be expressed by the following:

$$-\mathrm{d}M_{\mathrm{FeS2}}/\mathrm{d}t = \mathrm{d}M_{\mathrm{Fe}}/\mathrm{d}t = 0.5\mathrm{d}M_{\mathrm{SO4}}/\mathrm{d}t$$

where the molar rate ($\mathrm{d}M_{\mathrm{FeS2}}/\mathrm{d}t$) is negative since the reactant is being destroyed.

It is apparent from the reaction stoichiometry that the pyrite oxidation rate can be determined from measuring either the release rate of total dissolved iron or twice the release rate of total dissolved sulfate. Iron was chosen as the rate-determining variable because it would have been very difficult to discern analytically between the high background sulfate already present in the synthetic seawater matrix and the sulfate released from pyrite. In the absence of any Fe secondary phase precipitation, the total iron release rate per unit time, C t^{-1}, can thus be stoichiometrically equated to the pyrite oxidation rate:

$$-\mathrm{d}M_{\mathrm{FeS2}}/\mathrm{d}t = \mathrm{d}M_{\mathrm{Fe}}/\mathrm{d}t$$

so that each mole of FeS_2 that dissolves results in one mole of aqueous Fe being released into the seawater matrix.

An experimental approach has been taken to measure the rate of pyrite oxidation in seawater at conditions relevant to seafloor sulfide mining and weathering, by reacting crushed pure pyrite mineral powders of known specific surface area with synthetic seawater at different values of pH, temperature, and dissolved oxygen concentration.

Sample Preparation

Sample Crushing

Coarse euhedral pyrite specimens from the Huaron mining district in Peru were broken up with steel rock hammers and then crushed in a SPEX 8500 Shatterbox ring & puck mill. The ring and puck were composed of tungsten carbide. No more than fifty grams of pyrite were added to the mill at a time to ensure the sample was pulverized evenly. After addition of the pyrite sample the shatterbox was pulsed three times for thirty seconds each. Short runs on the shatterbox prevented the pyrite samples from being crushed too finely and reduced the chance of overheating the motor.

Immediately after pulverization the pyrite powder was sieved and separated according to grain size. Any pyrite grains larger than 150 microns were collected and run through the shatterbox an additional time. Pyrite grains less than 150 microns in diameter were collected in sealed glass jars. The powder containing

grains <150 microns was further crushed by hand using a ceramic mortar and pestle and sieved again to select grains that fell within the desired grain size range of 45-106 microns. This grain size range was selected because it yielded reaction rates with measurable dissolved iron products over several days or less. The final powder was then stored in sealed glass jars within a desiccator until the day of an experiment.

Importance of Cleaning/SEM Pictures

The sieved pyrite samples were cleaned chemically and ultrasonically immediately prior to experiments to remove extremely fine pyrite dust on the surfaces and expose fresh bulk surfaces on the mineral grains. An SEM photomicrograph (Figure 9) of pyrite before cleaning highlights the importance of the cleaning procedure. Upon crushing very fine particles of pyrite, down to 1 μm in diameter, remain adhered to the surfaces of the larger grains. Since the proposed rate law is dependent upon mineral specific surface area it is important to remove any adhering pyrite grains that do not fall within the specified grain size range of 45-106 μm. The microscopic pyrite particles have much greater specific surface areas than the larger grains to which they are attached and will therefore oxidize more rapidly, greatly distorting the true rate of the measured grain size range (McKibben, 1984).

Figure 9 also shows sharp edges and pointed corners on the surface of crushed pyrite grains. Such high-energy sites, as well as dislocations and defects,

represent locations where surface reactions such as oxidation are concentrated. Lüttge and Arvidson (2008) found that dislocation-free surfaces are substantially less reactive than surfaces containing distinct edges or corners. McKibben (1984) warned that oxidant attacks on the pyrite surface would not be evenly distributed across the mineral surface. These factors further indicate the importance of cleaning and minimizing mineral surface imperfections and adherences that could artificially enhance the oxidation rate.

Sample Cleaning

The following cleaning procedure developed by McKibben & Barnes (1986) was employed after minor modification. Six grams of sieved pyrite powder and approximately 40mL of pure ethanol were added to a 100mL glass beaker. The beaker was then placed in a Branson 3200 Ultrasonic Cleaner bath. Ultrasonic waves reverberating within the bath caused the fine-grained particles to detach from the larger pyrite grains, where they then became suspended within the ethanol. Carefully decanting the cloudy ethanol removed the fine particles while the large grains remained in the beaker. This process was repeated fifteen more times, or until the final decanted ethanol was substantially less cloudy than after the first ultrasonic wash. The efficiency of this technique in removing the fine particles seen in Figure 9 is made evident in an SEM photomicrograph taken after cleaning (Figure 10).

After the final ultrasonic wash, the pyrite was soaked in 1M HNO_3 for one minute. The acid soak dissolved sharp edges and minimized pit dislocations on the freshly cleaned pyrite surfaces. After the brief acid soak the grains were rinsed with 18.2 megaohm ultrapure water and, using pure ethanol in a wash bottle, were transferred from the beaker to the vacuum apparatus. Using ethanol to transfer the pyrite to the vacuum was advantageous because of ethanol's low vapor pressure relative to water; the drying time was nearly quartered from drying water-soaked grains. It also prevents water and air from starting to oxidize the freshly-prepared mineral surfaces. Once the pyrite sample had dried in the vacuum apparatus for approximately 90 seconds it was enclosed in a sealed glass jar and stored within a desiccator until the experiment was initiated. Pyrite samples were always cleaned within two hours of the start of an experiment.

Experimental Design

Reaction Vessel

"The chemical reactor must be regarded as the very heart of a chemical process."
C.G. Hill, 1977

Chemical kinetics experiments often utilize one of two types of broadly defined chemical reactors: the tank and the tube (Hill, 1977). Ideal tank reactors, the simpler of the two types, are containers in which the composition and temperature of the fluid are uniform throughout the vessel due to efficient stirring. There are three styles of tank reactors: batch, semi-batch, and continuous flow. The batch

reactor design was chosen for this pyrite oxidation study, both for its convenient size and ability to maintain a well-mixed, uniform composition at constant temperature for the duration of a run. It is best suited for the initial rate kinetics method as described below, and facilitates the analytical detection of accumulated reaction products for slow rates. All reactants within the batch reactor were closed off from the atmosphere.

The main disadvantage of the batch reactor is that dissolved reaction products can eventually precipitate as they build up in solution, limiting the conditions under which the rate can be easily measured. Use of a continuous flow reactor would avoid such complications, and also has the advantage of bringing a fresh supply of unreacted seawater to the pyrite surfaces. However, the high volumes of accumulating effluent seawater that have to be generated for continuous flow mode creates problems of high reagent costs, waste disposal and the challenge of analytical detection of dissolved reaction products at progressively more diluted concentrations.

The initial rate method (a type of regression analysis) discussed by Lasaga (1998) and utilized by McKibben and Barnes (1986) was combined with the method of isolation to determine the effects that temperature, pH, and dissolved oxygen concentration had on the oxidation rate. In the initial rate method the concentrations of a reaction product are measured through time and the results are graphed on a scatter plot. The first derivative of the resulting data curve, evaluated at $t = 0$, yielded the initial rate for that specific run. The isolation method allowed for

each parameter (pH, T, O2) in the rate law to be separately tested so that its individual influence on the rate would be explicated. This was accomplished by modifying the general form of the rate law into a linear regression equation, where the y-term in the equation represented the initial rate and the slope represented the rate's dependence on a specified condition. A full description of this methodology is discussed in the Sample Analysis section.

A 1.8-liter PTFE (Teflon) cylinder was chosen as the reaction vessel. PTFE is an ideal material for use as a reaction vessel because it is chemically inert and resistant to scratching and pitting, which allowed for each reaction vessel to be cleaned and reused hundreds of times with little concern for contaminants harboring within surface defects. Teflon is also a superb insulator. The seawater used in low and high temperature experiments required temperature conditioning before each run. This was accomplished within a temperature-controlled bath during the two-hour pre-experiment oxygen purge.

Figure 11 depicts a schematic cross section of the assembled reaction vessel used in experiments. Pyrite grains were constrained between double layers of 30 μm-opening, nylon mesh filters inside a threaded fitting sample holder that was suspended within the vessel by Plexiglas fins. 1 cm diameter ports with threaded caps in the top of the vessel allowed for collection of samples and temperature measurements without the need for completely opening the reaction vessel (Figure 12). All but the top of the Teflon reaction vessel was submerged within a 7.5 gallon temperature-controlled bath (Figure 13) during the experiment runs. The bath was

filled with antifreeze and topped off with hollow 2 cm diameter polyethylene spheres to maintain constant temperature during the 60-hr runs.

A Masterflex L/S peristaltic pump circulated synthetic seawater within the batch reactor in order to maintain a consistently well-mixed solution and surface-reaction-controlled conditions during experiments. The pump required 18-gauge tubing; a peroxide-treated silicone variety was utilized.

A maximum seawater pump rate averaging 2.5 L min^{-1} was employed to ensure that sufficient reactants were continuously fed to the surfaces of the pyrite grains based on the results of Bilenker (2011) and Romano (2011), to insure that the reaction rate measured was the mineral surface area-controlled rate and not one limited by rates of reactant transport in solution (Lasaga, 1998).

The specific surface area of the pyrite grains was measured using the BET gas adsorption method. Particle Tech Laboratories in Downers Grove, Illinois analyzed the surface area using a triple point Kr gas analysis. The specific surface area was 0.0332 ± 0.0010 m^2 g^{-1} for cleaned pyrite within the 45-106 μm grain size range.

Seawater Preparation

A synthetic seawater recipe published by Millero (2005) and used by Bilenker (2011) and Romano (2011) was also used in this study.

Pyrite was oxidized under acidic conditions primarily because of the limitations of the batch reactor design, but also due to the dependence of ferric ion solubility on pH and the natural acidic conditions that can occur near active seafloor

sulfide vent sites. Singer and Stumm (1970) found that ferric ions are soluble in solutions less than or equal to pH 4.5 while ferrous ions are soluble in water regardless of pH. Preventing ferric oxyhydroxide precipitation ensured that all iron released from pyrite oxidation remained in solution and was therefore measurable on the mass spectrometer. This was accomplished by acidifying each 2 L flask of artificial seawater with approximately 1.5 mL of 12M trace metal grade HCl. Acidifying the artificial seawater proved to be relevant for the application of this study since the pH of seawater surrounding active SMS fumaroles varies from 2 – 6 (Von Damm, 1995).

Sample Analysis

ICP-MS and SigmaPlot Analyses

On average, twenty-four 1 mL liquid samples were collected during each run via micropipette, using a sampling port in the top of the reaction vessel. These samples were then diluted with 2% trace metal grade HNO_3 and analyzed for total dissolved iron using the mass 56 isotope on an Agilent 7500 Series ICP-MS. Standard concentrations of 0, 2, 4, 6, 10, and 15 parts per billion Fe were utilized. Standards were prepared well in advance of mass spectrometer runs and each set of standards could be used to analyze around fifteen individual run sample sets.

The samples required at least a 9-fold dilution because seawater proved to be a corrosive matrix for the ultrasensitive ICP-MS. Initially a 15-fold dilution was employed but these samples proved to be too diluted for a reliable analysis.

The data gathered from the mass spectrometer required conversion from raw counts sec^{-1} to moles of iron. Once the raw data was converted to moles of iron a simple scatter plot of iron concentration versus time was created on Excel. These simple plots were the first opportunity to see if each experimental run was a success. The first graphs in Appendix B show typical run results in Excel scatter plot.

Data from successful runs were loaded into the computer graphing software SigmaPlot (version 11.0). A second-order polynomial regression equation was fit to the data and the equation for this curve was extracted using SigmaPlot.

Quadratic data curve: $\frac{C}{t} = ax^2 + bx + z$

Take the first derivative: $\frac{dC}{dt} = 2ax + b$

Evaluate at t = 0 $\left.\frac{dC}{dt}\right|_0 = b$

The first derivative represents the equation of the line tangent to the data plot at the given point. The slope of the tangent line defines the instantaneous rate of change in iron concentration at a specified time. Evaluating the first derivative at time equal to zero allows for the initial rate to be determined.

A rate law is a mathematical expression that can be used to quantify the rate of a chemical reaction. A general form of the rate law for pyrite oxidation is taken from Bilenker (2011) and Romano (2012), which was modified from McKibben *et al.* (2008). Rate laws typically cannot be estimated using the stoichiometric coefficients of reactants in an overall chemical reaction such as Equation 1, because the overall

reaction may be comprised of multiple intermediate reaction steps, one of which may be rate-limiting. Rate laws can only be determined through experimentation.

A general form of the rate law can first be expressed volumetrically:

$$R_{vol} = k\frac{SA}{V}[H^+]^a[P_{O_2}]^b$$

Where the rate constant k is a function of temperature, SA V^{-1} refers to the ratio of pyrite surface area (in m^2) to volume of seawater (in L), and the rate R is in units of moles L^{-1} sec^{-1}. The terms in brackets are the molal concentrations of protons and dissolved oxygen, while a and b are the orders of reaction for each reactant. The volumetric rate can be converted to the molal specific rate by dividing both sides of the rate law by the SA V^{-1} ratio:

$$R_{sp} = k[H^+]^a[P_{O_2}]^b$$

which is in units of moles m^{-2} sec^{-1}.

The initial rate method was combined with the isolation method to solve for the rate constant k as well as the unknown reaction orders a and b. Taking the logarithm of the generalized rate law and isolating a rate-controlling variable (either H^+ or P_{O2}) yields a simple linear regression equation. For example, if all conditions (T, SA V^{-1}, P_{O2}) except for pH are held constant for a series of runs, and the initial rate R is measured at different pH values, the value of the reaction order a can be determined from a plot of log R versus pH as follows:

$$\log R = \log k + a\log[H^+] + b\log[P_{O_2}]$$

$$\log R = a\log[H^+] + N$$

$$y = mx + b$$

The slope of the line represents the unknown reaction order for that specific rate-controlling variable, which mathematically describes the extent of dependence the overall oxidation rate has on that specific condition. The variable N is a constant.

Salting-Out Effect & Dissolved Oxygen

The influence that dissolved ions have on the solubility of a gas within a solution is called the "salting out" effect. The salting out effect predicts that less gas can remain dissolved in a solution that has a high ionic strength, such as seawater. This is due to the dissolved ions literally forcing the gas molecules out of the solution because there isn't enough room for the gas molecules to remain dissolved.

Benson and Krause (1984) published a detailed study in which they calculate the true concentration of dissolved oxygen in seawater at various temperatures and salinities under atmospheric pressure. The authors highlight the complexity involved in such calculations because of the various effects that salinity, temperature, and atmospheric pressure have on gas solubility within seawater. The researchers found temperature to be the most important factor in determining the amount of oxygen that can remain dissolved in seawater.

Dissolved oxygen concentrations were measured in mg L^{-1} by a Yellow Springs Instrument 85 D.O. meter. The D.O. meter was conditioned with a wet sponge and calibrated by inputting the lab's elevation above sea level. Average oxygen concentration in 20°C seawater after saturating with 0.995 atm oxygen gas

for two hours varied between 7.8 – 8.5 mg L^{-1}. This range corresponded to those dissolved oxygen values in pure seawater as calculated by Benson and Krause (1984), which are provided in Figure 14.

Pyrite Oxidation via Ferric Iron

This study did not investigate ferric iron's influence on the rate of oxidation. Data from this study suggests that ferric iron only plays a role in the instantaneous initiation of pyrite oxidation. In seawater at its normal pH, ferric iron immediately forms hydroxide species due to the ions high charge density compared to ferrous iron. In the example of an SMS deposit, any ferric minerals present near an active fumarole may dissolve and the iron would become reactive. As soon as the dissolved iron encountered pH 8 seawater, it would immediately precipitate out as a mineral or intermediate hydroxide species. Millero and Sotolongo (1989) determined the average Fe(III)/Fe(II) ratio in seawater to be <0.001 for over 190 samples in four oceans. Their ratio suggests that ferric ions available for pyrite oxidation may be limited in natural settings. Though ferric ions are present in seawater, they are not available to react unless the pH of the seawater is below 4.5. The effect that ferric iron has on the overall pyrite oxidation rate in non-acidic seawater is likely negligible.

Results

Experiments were conducted to determine the effects of pH, dissolved oxygen concentration, and temperature on the rate of pyrite oxidation in artificial seawater. Total dissolved iron was chosen as the rate-determining variable. The method of isolation was combined with the initial rate method to determine the rate dependence on each condition. Length of experimental runs varied depending on the condition being tested, with low oxygen runs lasting the longest at 60 hours. The oxidation reaction behaved congruently under low pH conditions (pH < 4.5) and high dissolved oxygen concentrations, regardless of temperature. Relevant data for all runs used to determine the rate law are provided in Appendix A while all scatter plots of runs are provided in Appendix B.

The derived rate law for pyrite oxidation in artificial seawater, as expressed volumetrically, is given by:

$$R_{vol} = -10^{-12.75\pm0.03}\,\frac{0.0664m^2}{1.8L}\,[H^+]^{0.39\pm0.03}[P_{O_2}]^{0.44\pm0.05}$$

in units of moles L^{-1} sec^{-1}. The surface area is doubled from the BET value because two grams of pyrite were oxidized per reaction vessel for each experiment. The molal specific rate law is given by:

$$R_{sp} = -10^{-11.02\pm0.03}[H^+]^{0.39\pm0.03}[P_{O_2}]^{0.44\pm0.05}$$

where R_{sp} is in units of moles m^{-2} sec^{-1}.

The following table (Table 1) lists linear regression equation parameters and the run conditions for all experiments used in determining the rate law. These

parameters were extracted from second-order polynomials fit to experiment run data. Quadratic curves of the form: $C\ t^{-1} = bx^2 + ax + y_0$ for each run are provided on scatter plots in Appendix B. Runs labeled with "D" are duplicates of the run above them.

Run	b	a	y_0	Std Error (a)	SA (m^2)	pH	P_{O2} (atm)	temp (K)	SA V^{-1} ratio
2J	-2.2289E-20	4.177E-14	1.954E-10	1.2146E-15	0.0332	2.05	0.995	293	0.018444
2K (D)	-7.2682E-20	3.8985E-14	1.9654E-10	1.4639E-15	0.0332	2.05	0.995	293	0.018444
2L	-1.8979E-20	2.3988E-14	9.9417E-11	4.0556E-15	0.0332	2.92	0.995	293	0.018444
2M (D)	-4.4671E-20	2.2909E-14	1.4295E-10	6.4351E-15	0.0332	2.92	0.995	293	0.018444
2H	-7.3327E-20	1.9841E-14	2.2514E-10	1.3185E-15	0.0332	3.51	0.995	293	0.018444
2I (D)	-6.0611E-20	2.0045E-14	2.4947E-10	1.2481E-15	0.0332	3.52	0.995	293	0.018444
2A	-3.5823E-20	9.1153E-15	1.6008E-10	6.8291E-16	0.0332	4.04	0.995	293	0.018444
2B (D)	-5.0664E-20	1.3138E-14	1.4132E-10	5.9596E-15	0.0332	4.01	0.995	293	0.018444
1I	-3.6063E-19	3.9008E-15	1.0744E-10	3.7443E-16	0.0332	4.54	0.995	293	0.018444
1J (D)	-3.9955E-19	3.9811E-15	1.0922E-10	3.8784E-16	0.0332	4.54	0.995	293	0.018444
X	-4.0057E-19	3.0559E-15	1.4202E-10	6.9458E-16	0.0332	5.05	0.995	294	0.018444
3A	-2.3718E-20	1.4317E-14	2.0713E-10	8.5434E-15	0.0332	2.47	0.1	295	0.018444
3B (D)	-1.1063E-20	1.0786E-14	1.0084E-10	6.0809E-15	0.0332	2.47	0.1	295	0.018444
2W	-7.6868E-21	1.1423E-14	7.2586E-11	3.0195E-15	0.0332	2.55	0.1	294	0.018444
2X (D)	-3.2508E-20	1.2279E-14	6.5435E-11	2.7204E-15	0.0332	2.55	0.1	294	0.018444
3H	-1.4322E-20	8.0594E-14	6.0035E-11	4.6183E-15	0.0332	2.51	0.995	285	0.018444
3I	-3.3804E-20	5.479E-14	5.0271E-11	7.0588E-15	0.0332	2.54	0.995	303	0.018444

Table 1: Linear regression parameters used in the rate law

The experimental derivation of the rate constant and the reaction orders for each rate-controlling variable in the rate law are described below.

Effect of pH

Experiments were conducted to determine the influence of pH on pyrite oxidation in acidic seawater. Every half unit between pH 2 – 5 was tested at 293 K, 0.995 atm oxygen, and a constant SA V^{-1} ratio. Figure 15 depicts a plot of log (oxidation rate) versus log (proton concentration). The data plot reveals a partial-order dependence of the rate on initial pH conditions. The slope of the line is 0.39±0.02, nearly four times more than the value reported by McKibben (1984) for pyrite oxidation in acidic aqueous solutions when oxygen is the sole oxidant (m_{pH} = 0.09). This would suggest that pH plays a larger role in the oxidation of pyrite in acidic seawater than in acidic sterile waters.

Figure 15 was created using data collected from low pH runs less than or equal to pH 5. It was not expected that iron-bearing minerals and intermediate species would precipitate during the runs since ferric iron is soluble in acidic (pH < 4) aqueous solutions. To show the effects at higher pH, Figure 16 depicts two pyrite samples on the sample-containing mesh immediately after oxidation experiments. The unmarked sample on the top underwent a 50-hour run at pH 2.5, 0.995 atm O_2, and 293 K. Following the run the pyrite looked unreacted and no precipitates were visible. This was very common for experiments run under similar conditions. The pyrite on the bottom was oxidized for a 50-hour run at pH 6, 0.995 atm O_2, and 293 K and clearly became discolored during the run. Figure 17 also depicts pyrite on the

sample mesh but from a 40-hour run at pH 8.2, 0.995 atm O_2, and 293 K. An orange precipitate, likely Fe(III) hydroxide, has been deposited on the mesh. Oxide staining was not observed after runs that used acidic seawater.

Effect of Dissolved Oxygen Concentration

A series of experiments was conducted to determine dissolved oxygen's influence on the abiotic rate of pyrite oxidation. Two distinct concentrations of oxygen, a nearly pure, 99.5% concentration and a 10% mixture balanced with nitrogen, were used to determine this influence. Figure 18 depicts a plot of log (oxidation rate) versus log (oxygen concentration). The order of reaction determined from the slope of this line is 0.44 ± 0.04, which signifies an oxidation rate dependence of less than the square root of the initial dissolved oxygen concentration (McKibben, 1984). The reaction order of 0.44 shows that the initial dissolved oxygen concentration is slightly more influential on the pyrite oxidation rate than the initial pH of the seawater (0.39), similar to the findings of Bilenker (2011) and Romano (2011).

McKibben (1984) explained his oxygen square root rate law in terms of a reaction mechanism. He proposed that water molecules on the pyrite surface would react with dissolved oxygen to form an intermediate hydrogen peroxide species, which was then able to oxidize the pyrite sulfur to sulfate. Oxidation of sulfur via the hydroxide species, he argues, is the rate-limiting step in the oxidation of pyrite by dissolved oxygen (McKibben, 1984).

Effect of Temperature

The following table (Table 2) lists ln(k) values, their errors, and T^{-1} values for those experiments which tested the effect of temperature on the pyrite oxidation rate in acidic seawater. The average ln(k) values were graphed against the inverse absolute temperature on an Arrhenius plot. Standard deviation values were calculated on Excel.

Experiment	Temperature (K)	ln(k)	Average ln(k)	STD Deviation	STD Error	T^{-1}
3G	285	-25.879	-25.893	0.0197	0.0139	0.00351
3H (D)	285	-25.907				
2L	293	-25.457	-25.439	0.0249	0.0176	0.00341
2M (D)	293	-25.421				
3I	303	-24.969	-24.986	0.024	0.0169	0.0033
3J (D)	303	-25.003				

Table 2: Parameters graphed in Arrhenius Plot (Figure 19)

An Arrhenius plot (Figure 19) was used to determine the effect of temperature on the reaction rate. Initial pH (3.00±0.05), dissolved oxygen concentration (0.995 atm), and the SA V^{-1} (0.018444) ratio were held constant for experiments ran at 285, 293, and 303 K. The activation energy E_a of pyrite oxidation in seawater was calculated from the T^{-1} vs. ln(k) plot by using the Arrhenius equation:

Equation 5. $k = Ae^{-Ea/RT}$

The E_a was calculated as 37.08 kJ mol^{-1}. The activation energy for pyrite oxidation in acidic seawater was significantly lower than the 56.9 kJ mol^{-1} value calculated by McKibben (1984) for pyrite oxidation in acidic sterile water. The slope of the line T^{-1} vs. ln k remains nearly constant across the three distinct temperature values. This suggests that the activation energy for pyrite oxidation in acidic seawater would remain consistent across a range of low temperatures.

Discussion

Previous sulfide oxidation kinetics studies performed by Bilenker (2011) and Romano (2011) yielded rate laws for chalcopyrite and pyrrhotite oxidation in artificial seawater, respectively. The pyrite dissolution rate in seawater was quite slow compared to the other sulfide minerals. In many runs the measured iron release rate from pyrite was nearly twenty times slower than the iron release rate

from Bilenker's chalcopyrite. The molal concentration of iron released from pyrite (even after 2.5 days) never surpassed 12 ppb, regardless of the run conditions. Shorter runs (~8 hrs) oxidizing pyrrhotite yielded iron concentrations that averaged 5 ppm, nearly three orders of magnitude greater than pyrite (Romano, 2011). Therefore pyrite oxidizes the slowest of the three sulfide minerals in low temperature, acidic seawater.

The rate law's dependence on both the initial pH and dissolved oxygen concentration are represented by the fractional reaction orders 0.39 and 0.44, respectively. These values suggest that both conditions are not very influential on the oxidation rate, at least not in the low pH range of 2 – 5.

In order to quantify the risk of localized ocean acidification associated with seafloor sulfide mining, one may consider the buffer capacity of seawater. Thompson and Bonnar (1931) published the following equation which relates seawater buffer capacity (B_C) to its chloride content (Cl^-) in grams.

Equation 5. $B_C = 0.1252(Cl^-)$

From the Millero (2005) recipe, 19 grams of Cl^- are dissolved in every kilogram of seawater. Therefore synthetic seawater used in experiments neutralizes up to 2.38 grams of acid per kilogram of seawater. If the pyrite dissolution reaction behaves according to the reaction stoichiometry in Eq. 1, then two moles of acid (H^+) are produced for every mole of pyrite that dissolves. Multiplying the moles of acid

produced by the molecular weight of H^+ (1.008 g mol^{-1}) yields 2.016 grams of acid, which is below the buffer capacity of seawater.

Implications for Seafloor Sulfide Mining

These findings, along with those published by Bilenker (2011) and Romano (2011), have positive implications for groups interested in exploiting SMS deposits for ore minerals. The findings of this study suggest that freshly crushed pyrite larger than 45 μm may not contribute to the localized acidification of the ocean near seafloor sulfide mining sites. The data shows that even in areas of active submarine hydrothermal venting, where the pH of seawater can drop to 2, pyrite will not oxidize fast enough for considerable amounts of sulfuric acid to be generated.

The slow pyrite oxidation rate, over considerable time, may lead to a concentration of pyrite in extinct hydrothermal vent systems. This could prove problematic to mining companies because pyrite is a gangue mineral; any pyrite the company encounters will only end up costing them more money. Taylor *et al.* (1995) found that pyrite was the dominant sulfide mineral found in VMS deposits, suggesting the preservation of pyrite in seafloor sulfides to be a widespread phenomenon. The volume of pyrite in a VMS deposit is rarely published since pyrite is a noneconomic mineral so a direct comparison between pyrite concentration in extinct VMS and active SMS deposits is difficult. Pyrite will survive weathering longer than other sulfides so it can be inferred that the pyrite to sulfide ratios of VMS deposits will be larger than the same ratios at SMS deposits.

One concern to deep-sea miners should be the fact that much of the effluent that will be injected back into the deep ocean could contain very finely crushed pyrite particles measuring less than 10 μm in diameter (Nautilus, 2014). A small grain size translates to a very large surface area, leading to that freshly ground, fine-grained pyrite to become highly reactive. Recall the volumetric rate law contains the SA V^{-1} ratio:

$$R_{vol} = k\frac{SA}{V}[H^+]^a[P_{O_2}]^b$$

Increasing the available mineral surface area while holding volume constant will increase the volumetric rate, leading to the production of more sulfuric acid. After being returned to the deep sea these extremely fine pyrite particles could remain suspended and float into the proximity of active hydrothermal vents where the pH is below 4. Such conditions would greatly exacerbate the slow rate measured in this study.

Conclusions

Several conclusions can be made considering the results of this study.

1. Pyrite oxidizes at a slower rate in seawater than the copper ore mineral chalcopyrite (Bilenker, 2011) and the iron monosulfide pyrrhotite (Romano, 2011).
2. The initial concentration of dissolved oxygen is more influential upon the initial pyrite oxidation rate than the initial pH of the seawater in acidic, low

temperature conditions (though this level of influence is only slightly greater than pH).

3. The activation energy (E_A) for pyrite oxidation in acidic seawater is 37.08 kJ mol^{-1}, and the linear nature of the Arrhenius Plot suggests that the E_A remains constant across a range of low temperatures.
4. The slow oxidation rate coupled with the sheer volume of acid-buffering seawater surrounding extinct fumaroles will not lead to significant changes in ocean pH as seafloor sulfide deposits are naturally weathered and anthropogenically exploited.
5. Active hydrothermal vent systems may intensify the oxidation rate of very fine pyrite particles that are returned to the deep ocean as waste slurry from the surfaces of ore mineral processing ships.

Future Work

Fortunately, as this is one of several preliminary studies on sulfide mineral oxidation kinetics in acidic seawater, the results suggest several possible avenues for future research. Consideration should be given towards the oxidation kinetics of those extremely fine particles of waste material that would be sent back to the ocean after processing on the ship. A study such as this may also shed light on the residence time of small mineral grains in the deep ocean. This research would require a bit of ingenuity as grains that small could not be contained in the same

batch reactor vessel sample containers utilized in the current study. It may help to investigate the general relationship between mineral oxidation rate and grain size.

Of course, studying the oxidation kinetics of other sulfide minerals, including sphalerite and galena, in seawater would be of great relevance. Investigating the same mineral (py, cp, po) reaction rates under high temperatures could produce interesting results, though the batch reactor may not serve as an ideal experimental design for this study due to expected higher evaporation rates.

References

Benson, B.B. and Krause, D., 1984. "The concentration and isotopic fractionation of oxygen dissolved in freshwater and seawater in equilibrium with the atmosphere" *Limnol. Oceanography* 29, p. 620-632.

Bethke, C.M., 2009. The Geochemist's Workbench® 8.0. www.gwb.com

Boschen, R.E., 2013. "Mining of Deep-sea Seafloor Massive Sulfides: A Review of the Deposits, Their Benthic Communities, Impacts from Mining, Regulatory Frameworks and Management Strategies." *Ocean and Coastal Management* vol. 84, p. 54-67.

Brantley S.L., Kubicki J.D. and White A.F., eds., 2008. *Kinetics of Water-Rock Interaction*. New York: Springer Science+Business Media, LLC.

Buxton, A., 2012. "MMSD+10: Reflecting on a decade of mining and sustainable development". International Institute for Environment and Development

Correia, J., 2010. "Red River 1" blog post on trekearth.com, accessed 4/26/15

DuPont (1996) "Teflon™ PTFE Properties Handbook". Accessed online 10/25/15

Garrels, R.M. and Thompson, M.E., 1960 "Oxidation of Pyrite in ferric sulfate solution." *American Journal of Science* vol. 258, p. 57-67

Gleisner, M., 2005. Quantification of mineral weathering rates in sulfidic mine tailings under water-saturated conditions. PhD Dissertation. Department of Geology and Geochemistry, Stockholm University, Sweden.

Herzig *et al.*, 2000, "Proceedings. Minerals other than polymetallic nodules of the international seabed area." Kingston, Jamaica: International Seabed Authority, p. 109-161

Hoagland, P., Beaulieu, S., Tivey, M.A., Eggert, R.G., German, C., Glowka, L., Lin, J., 2010. "Deep-sea mining of seafloor massive sulfides" *Marine Policy.*, 34, p. 728-732.

International Monetary Fund, 2016. World Economic Outlook Update, January 2016. "Subdued Demand, Diminished Prospects"

International Monetary Fund, 2016. World Economic Outlook Update, July 2016. "Uncertainty in the Aftermath of the U.K. Referendum"

Lasaga, A.C., 1998. Kinetic Theory in the Earth Sciences. Princeton, New Jersey: Princeton University Press.

Luther, G.W., 1987. Pyrite oxidation and reduction: Molecular orbital theory considerations. *Geochimica et Cosmochimica Acta* **51**, p. 3192-3199.

McKibben, M.A., 1984. "Kinetics of Aqueous Oxidation of Pyrite by Ferric Iron, Oxygen, and Hydrogen Peroxide from pH 1-4 and 20-40°C." Thesis. The Pennsylvania State University, Print.

Bilenker, L.D., 2011. Abiotic Oxidation Rate of Chalcopyrite in Seawater: Implications for Seafloor Mining. Unpublished Master's thesis, University of California, Riverside.

McKibben, M.A. and Barnes, H.L., 1986. Oxidation of pyrite in low temperature acidic solutions: Rate laws and surface textures. *Geochimica et Cosmochimica Acta 50*, 1509-1520.

McKibben, M. A., Tallant, B.A. and Del Angel, J.K., 2008. "Kinetics of inorganic arsenopyrite oxidation in acidic aqueous solutions." *Applied Geochemistry* 23.2, p. 121-135.

Millero, F.J., 2005. Chemical Oceanography, Third Edition. CRC Press

Millero, F.J. and Sotolongo, S., 1989. The oxidation of Fe(II) with H_2O_2 in seawater. *Geochimica et Cosmochimica Acta 53*, 1867-1873.

Nautilus Minerals, Ltd., 2008. "Environmental Impact Statement: Solwara 1 Project Executive Summary." Study performed by Coffey Natural Systems, pg. 1-50.

Nautilus Minerals, Ltd., 2014. "Fact Sheet Q2, 2014: Solwara 1 Seafloor Production System." pgs. 2-5, 14.

Nordstrom, D.K., 1982. "Aqueous pyrite oxidation and the consequent formation of secondary iron minerals." Acid Sulfate Weathering, p. 37-56, Soil Science Society of America

Nordstrom, D.K. and Alpers, C.N., 1999. "Geochemistry of acid mine waters." *The Environmental Geochemsitry of Mineral Deposits*. Reviews in Economic Geology 6A, Society of Economic Geologists, p. 133-160.

Radiga, M., 2013. "A trip to Mars" blog post on eyeonspain.com, accessed 4/26/15

Rimstidt, J.D., Chermak, J.A., and Gagen, P.M., 1993. "Rates of Reactions of Galena, Sphalerite, Chalcopyrite, and Arsenopyrite with Fe(III) in Acidic Solutions" *Environmental Geochemistry of Sulfide Oxidation*, ACS Symposium Series, American Chemical Society

Rimstidt J. D. and Newcomb, W.D., 1993. "Measurement and analysis of rate data: The rate of reaction of ferric iron with pyrite." *Geochimica et Cosmochimica Acta* **57**, p. 1919-1934.

Rimstidt, J.D. and Vaughan, D.J., 2003. "Pyrite oxidation: a state-of-the-art assessment of the reaction mechanism." *Geochimica et Cosmochimica Acta* **67**, p. 873-880.

Romano, G.Y., 2011. "Kinetics of Pyrrhotite Oxidation in Seawater: Implications for Mining Seafloor Hot Spring." Unpublished Master's thesis, University of California, Riverside.

Singer, P.C. and Stumm, W. 1969. "Oxygenation of ferrous iron." FWQA Rep. 14010-06/69

Singer, P.C. and Stumm, W., 1970. "Acidic Mine Drainage: The Rate-Determining Step." Science 20, p. 1121-1123.

Sweeney, R.E. and Kaplan, I.R., 1973. "Pyrite Framboid Formation; Laboratory Synthesis and Marine Sediments" Economic Geology August 1, 1973 vol. 68, no. 5, p. 618-634.

Taylor, C.D., *et al.*, 1995. "Volcanic-Associated Massive Sulfide Deposits." Preliminary Compilation of Descriptive Geoenvironmental Mineral Deposit Models. USGS Publications.

Thompson, T.G. and Bonnar, R.U., 1931. "The Buffer Capacity of Sea Water." *Ind. Eng. Chem., Anal. Ed.,* pg. 393

Tivey, M.K., 2007. "Generation of Seafloor Hydrothermal Vent Fluids and Associated Mineral Deposits." *Oceanography*, Vol. 20, No. 1

Von Damm, K.L., 1995. "Temporal and compositional diversity in seafloor hydrothermal fluids." *Reviews of Geophysics*, Vol. 33, Issue S2, p. 1297-1305.

Williamson, M.A. and Rimstidt, J.D., 1994. “The kinetics and electrochemical rate-determining step of aqueous pyrite oxidation” *Geochimica et Cosmochimica Acta*, Vol. 58 Issue 24 p. 5443-5454.

Figures

Figure 1. Rio Tinto in SW Spain; its red color is due to pollution from dissolved metals (Correia, 2010)

Figure 2. An extreme example of acid mine drainage in Rio Tinto, near a 1000 year old mining site in Spain (Radiga, 2013)

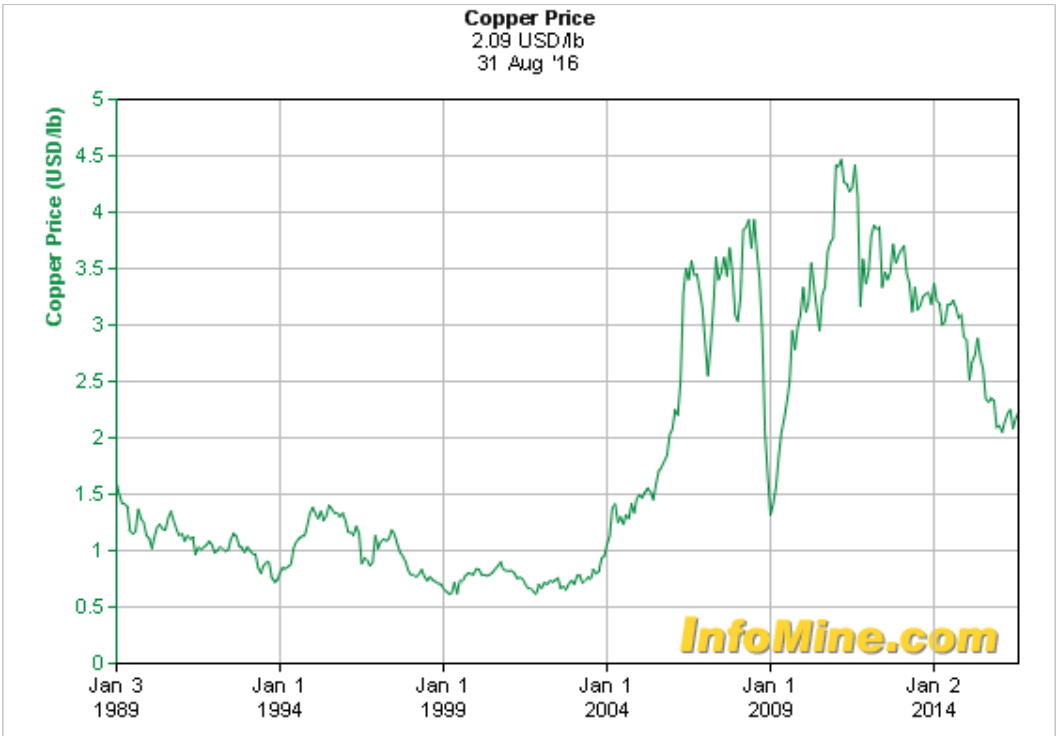

Figure 3. 25 year historical copper trading prices and current value as of 8/31/16

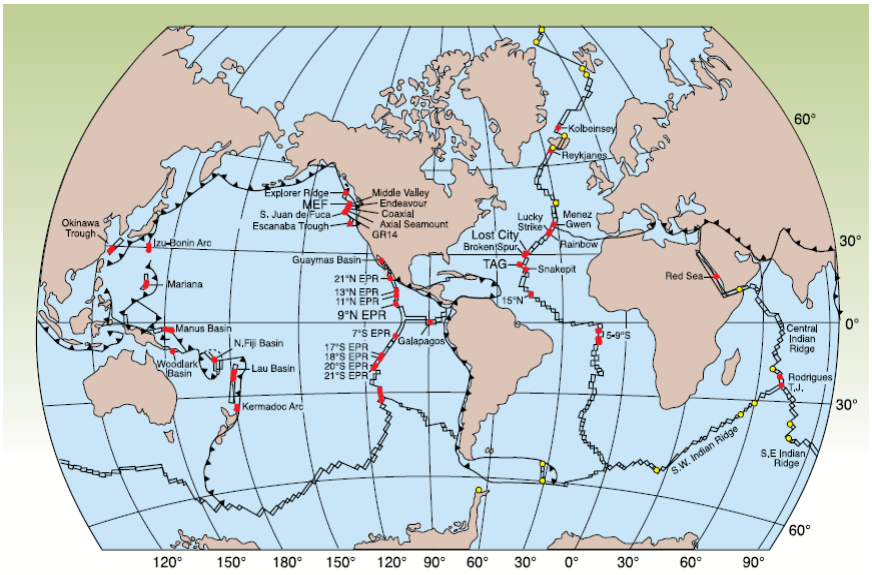

Figure 4. Map showing the global distribution of known (red) and inferred (yellow) SMS deposits. Note their occurrence in the back-arc basins and volcanic island chains of the western Pacific and along divergent plate margins worldwide. (Tivey, 2007)

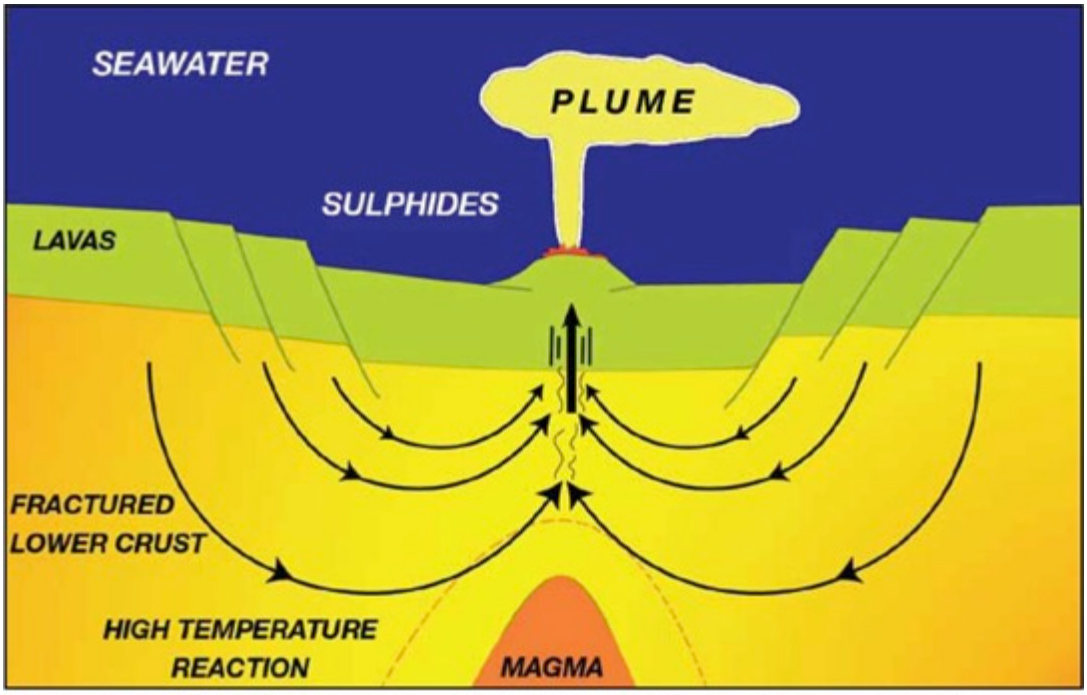

Formation of seafloor sulphides. (Herzig et al. Proceedings. Minerals other than polymetallic nodules of the international seabed area, Kingston, Jamaica: International Seabed Authority, 2000, pp. 109-161.)

Figure 5. Cross-section of hypothetical oceanic crust that details a possible formation mechanism of an SMS deposit. (Herzig *et al.*, 2000)

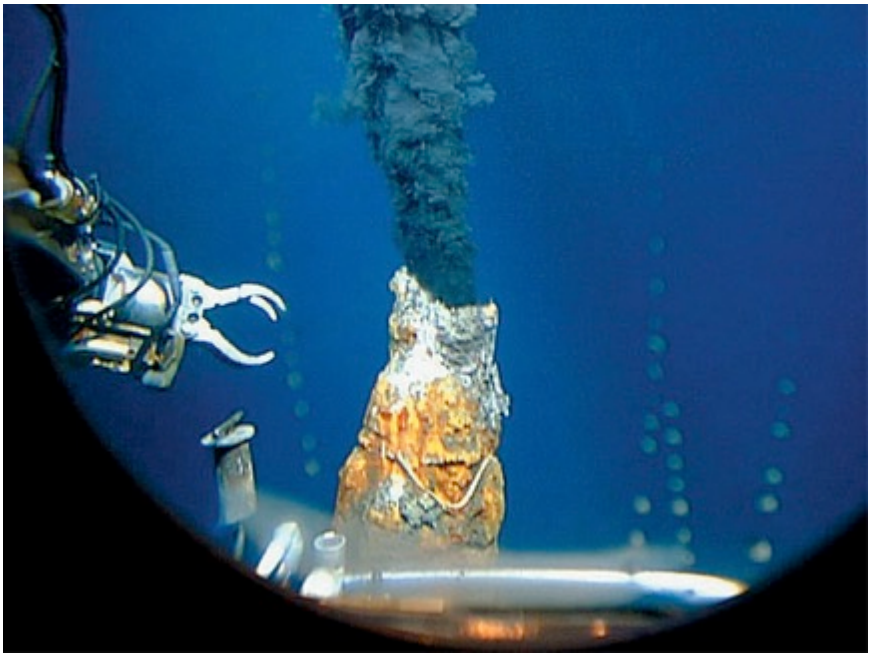

Figure 6. Submarine fumarole, an example of active seafloor massive sulfide hydrothermal vent as photographed by Nautilus Minerals, unknown location (2014)

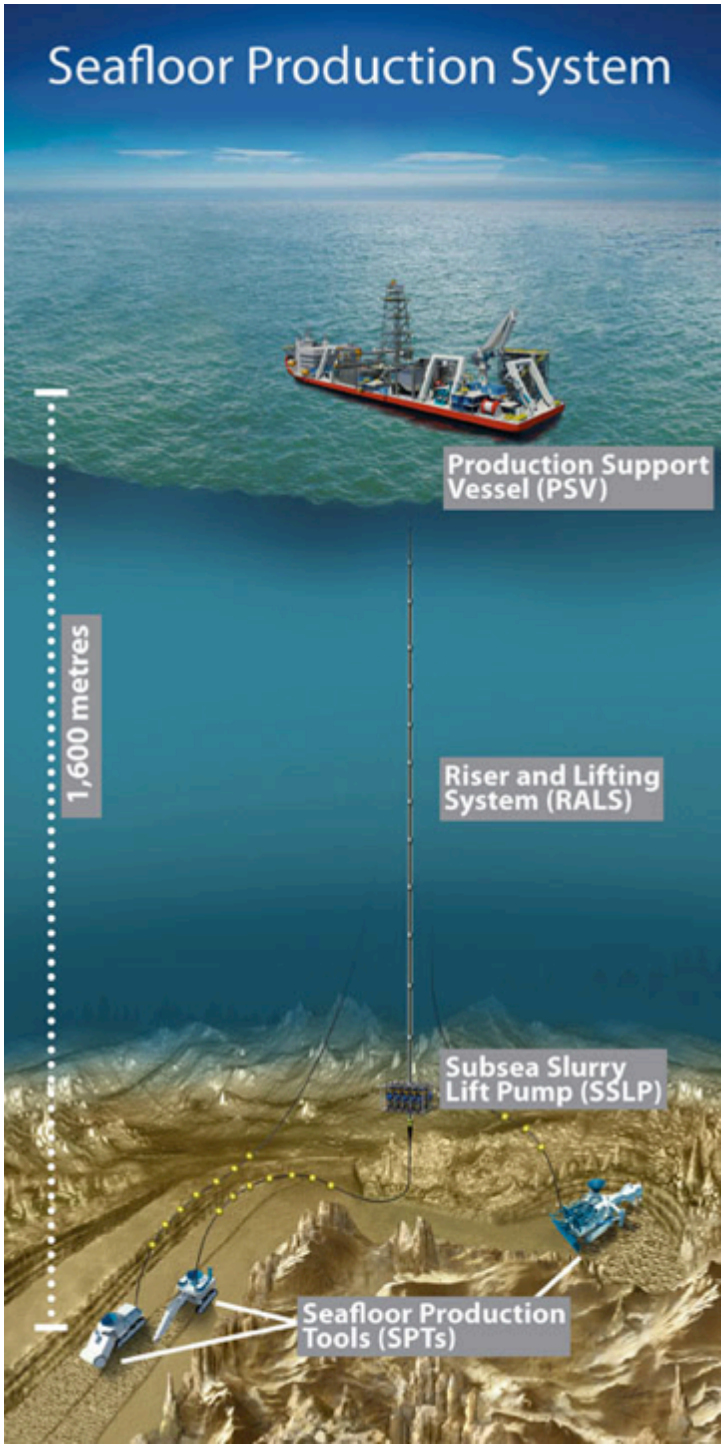

Figure 7. Multi-component ore recovery process proposed at Solwara-1 (first proposed SMS mining site) by Nautilus Minerals (2014)

Temp (K)	273	298	333	373	423	473	523	573
log(K)	239.68	217.40	190.96	166.09	140.59	119.49	101.13	84.39
ΔG^0 (kJ mol^{-1})	-12.44	-13.34	-14.54	-15.86	-17.39	-18.81	-20.08	-21.13

Figure 8. Table of equilibrium constants for specific temperatures determined by Geochemists Workbench (Bethke, 2009). The increasingly negative Gibbs free energy values show that as temperature increases the likelihood (spontaneity) of the pyrite oxidation reaction to occur also increases. ΔG^0 values determined by: $\Delta G^0 = -2.303RT[\log(K)]$

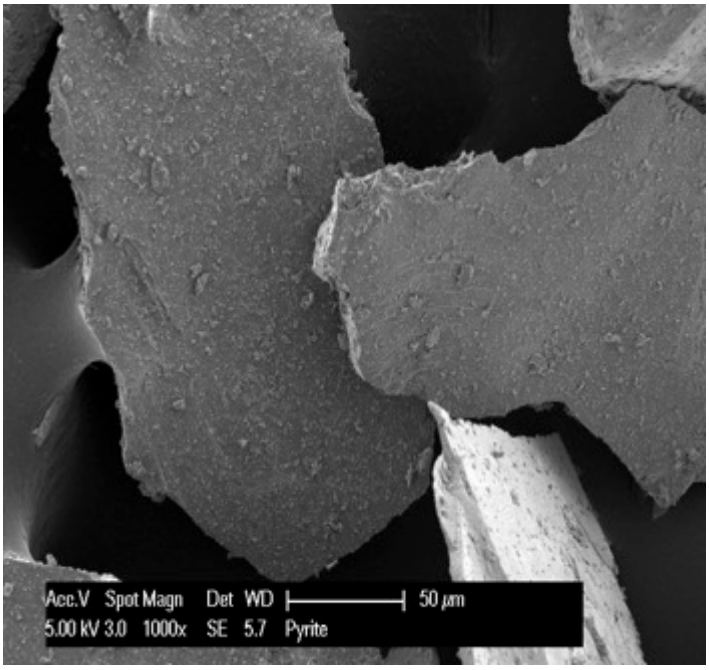

Figure 9. SEM photomicrograph of pyrite grains before cleaning. The dirty pyrite grains are coated in dust-sized particles of pyrite

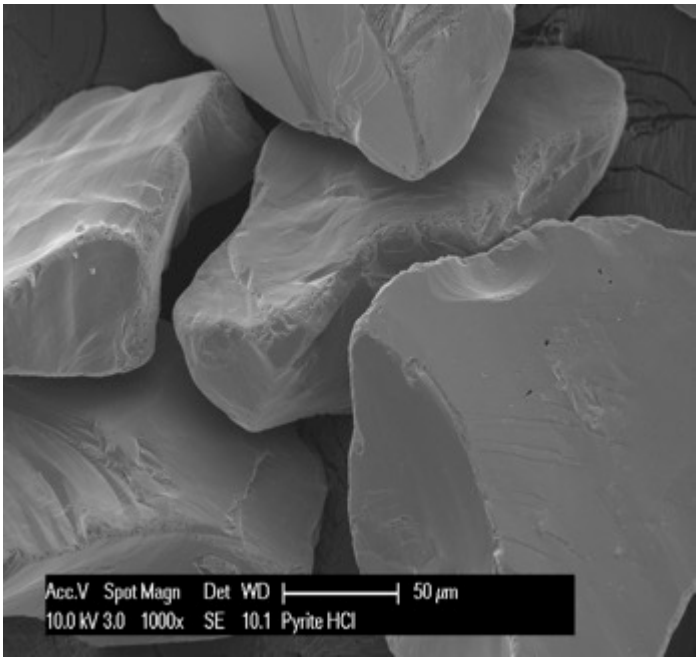

Figure 10. SEM photomicrograph of pyrite after cleaning with the modified procedure from McKibben (1984). Note the dust-sized pyrite particles have been removed from the surfaces of the sample grains.

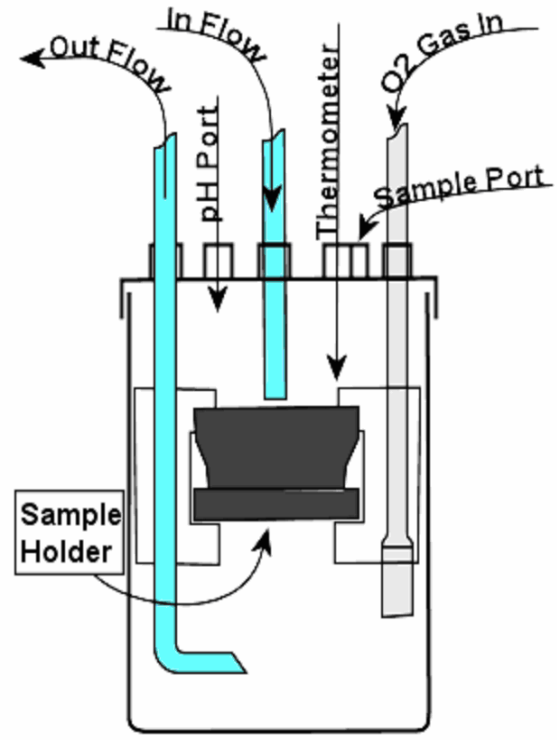

Figure 11. From McKibben *et al.* (2008). Schematic cross section of the assembled reaction vessel. It shows the location of the pyrite grain sample holder and the configuration of glass tubes used for seawater inflow and outflow, oxygen intake, sample collecting, and measuring temperature.

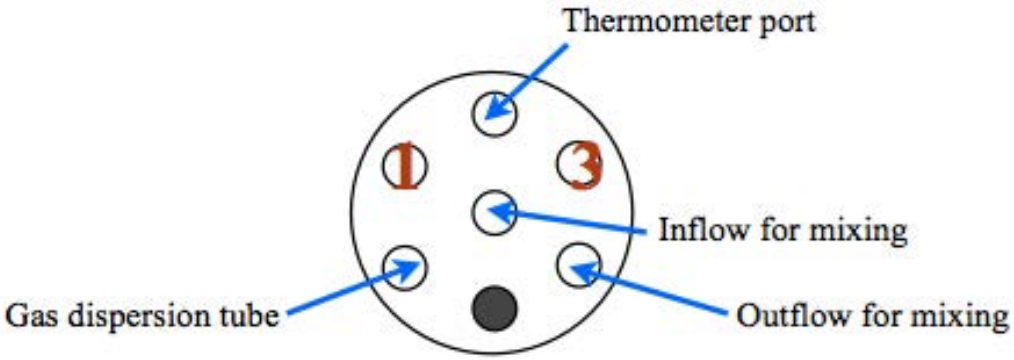

Figure 12. From Bilenker (2011). Aerial view of reaction vessel showing ports for inflow/outflow of seawater, collecting samples, and measuring temperature. Port labeled 3 was used to collect samples while port 1 was sealed.

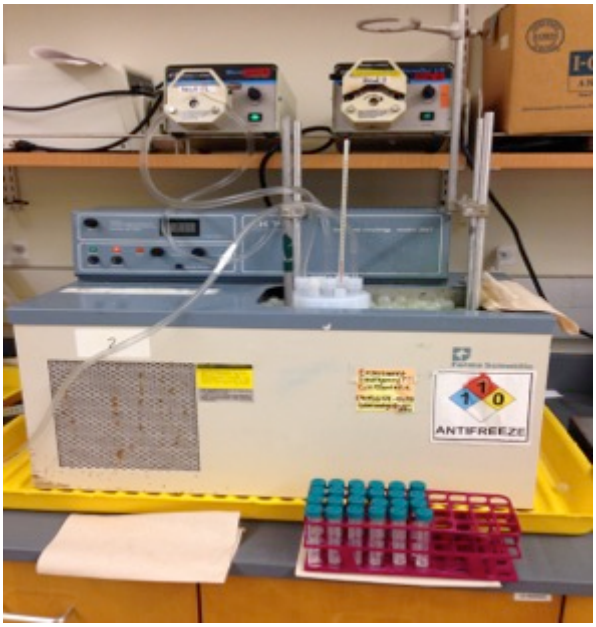

Figure 13. Forma Scientific (model 2067) temperature-controlled circulating bath filled with antifreeze and topped with Teflon spheres for insulation. Note the assembled reaction vessel sitting inside the bath and the Masterflex L/S peristaltic pump on overlying shelf.

Table 7. Values for C^*_O in mg·liter^{-1} at integral temperatures and intervals of five in salinity.

Temp (°C)	Salinity 0	5	10	15	20	25	30	35	40
0.0	14.621	14.120	13.636	13.167	12.714	12.277	11.854	11.445	11.051
1.0	14.216	13.733	13.266	12.815	12.378	11.956	11.548	11.154	10.773
2.0	13.829	13.364	12.914	12.478	12,057	11.650	11.256	10.875	10.507
3.0	13.460	13.012	12.577	12.157	11.750	11.356	10.976	10.608	10.252
4.0	13.107	12.674	12.255	11.849	11.456	11.076	10.708	10.352	10.008
5.0	12.770	12.352	11.947	11.554	11.175	10.807	10.452	10.107	9.774
6.0	12.448	12.043	11.652	11.273	10.905	10.550	10.206	9.872	9.550
7.0	12.139	11.748	11.369	11.003	10.647	10.303	9.970	9.647	9.335
8.0	11.843	11.465	11.099	10.744	10.400	10.066	9.744	9.431	9.128
9.0	11.560	11.194	10.839	10.495	10.162	9.839	9.526	9.223	8.930
10.0	11.288	10.934	10.590	10.257	9.934	9.621	9.318	9.024	8.739
11.0	11.027	10.684	10.351	10.028	9.715	9.412	9.118	8.832	8.556
12.0	10.777	10.444	10.122	9.809	9.505	9.210	8.925	8.648	8.379
13.0	10.537	10.214	9.901	9.597	9.303	9.017	8.739	8.471	8.210
14.0	10.306	9.993	9.689	9.394	9.108	8.830	8.561	8.300	8.046
15.0	10.084	9.780	9.485	9.199	8.921	8.651	8.389	8.135	7.889
16.0	9.870	9.575	9.289	9.010	8.740	8.478	8.224	7.976	7.737
17.0	9.665	9.378	9.100	8.829	8.567	8.311	8.064	7.823	7.590
18.0	9.467	9.188	8.917	8.654	8.399	8.151	7.910	7.676	7.449
19.0	9.276	9.005	8.742	8.486	8.237	7.996	7.761	7.533	7.312
20.0	9.092	8.829	8.572	8.323	8.081	7.846	7.618	7.396	7.180
21.0	8.915	8.658	8.409	8.166	7.930	7.701	7.479	7.262	7.052
22.0	8.743	8.494	8.251	8.014	7.785	7.562	7.345	7.134	6.929
23.0	8.578	8.335	8.098	7.868	7.644	7.426	7.215	7.009	6.809
24.0	8.418	8.181	7.950	7.726	7.508	7.295	7.089	6.888	6.693
25.0	8.263	8.032	7.807	7.588	7.376	7.169	6.967	6.771	6.581

Figure 14. Corrected dissolved oxygen values in pure seawater under standard atmospheric pressure and composition, as published by Benson and Krause (1984). Note the corresponding values ranging from 7.4 – 8.7 mg L^{-1} for the most commonly tested temperature range of this study (12 - 20°C). Average dissolved oxygen concentrations measured before runs (for T = 20°C) ranged from 7.8 – 8.5 mg L^{-1}.

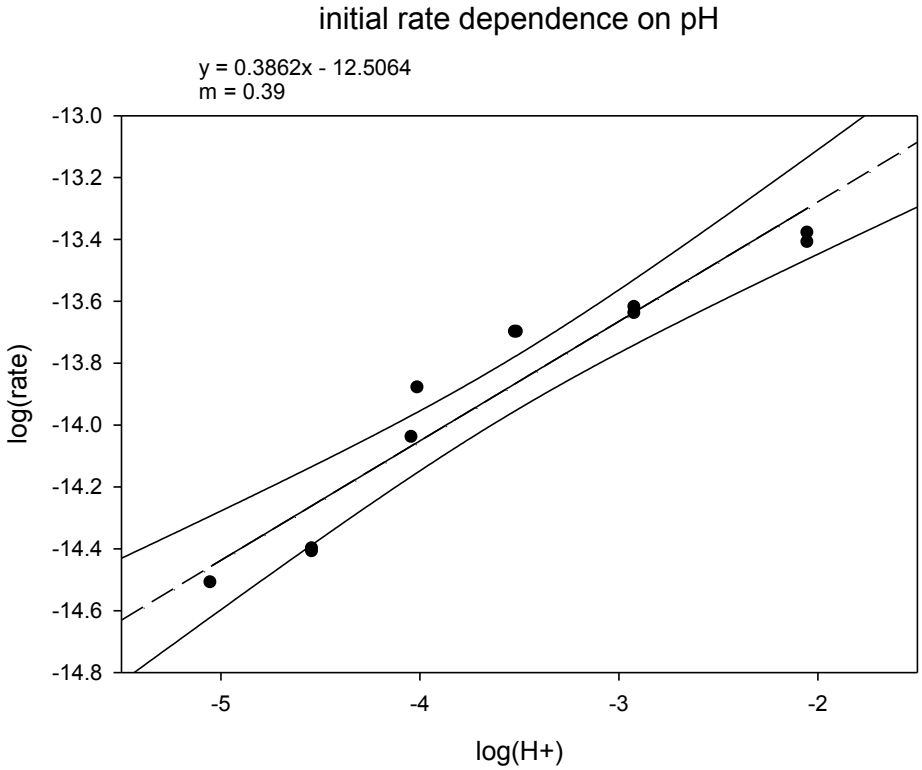

Figure 15. Graph showing the initial rate dependence on initial seawater pH, generated on Sigma Plot. The outer solid lines represent a 95% confidence interval.

Figure 16. Pyrite on the top (oxidized at pH 2) looks unreacted. Pyrite on the bottom (oxidized at pH 8.1) is discolored, suggesting an iron (Fe^{3+}) hydroxide formed directly on the surface.

Figure 17. Sample-containing mesh after an experiment run at pH 5.5; an iron oxide precipitate has stained the mesh. This phenomenon was never observed under acidic conditions.

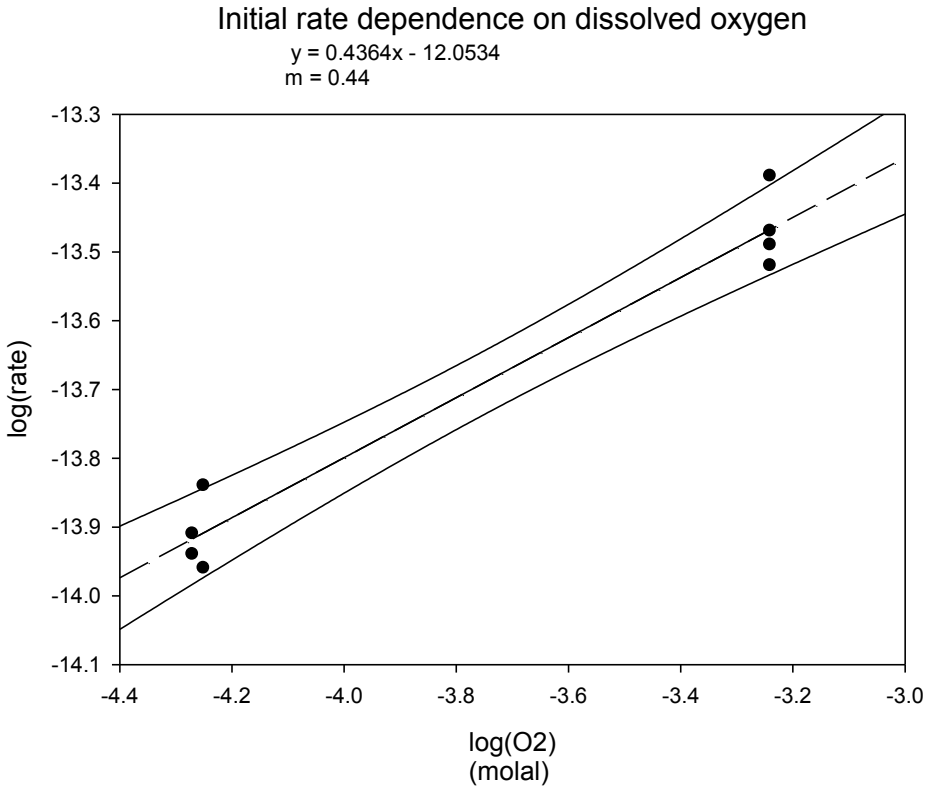

Figure 18. Graph showing the initial rate dependence on oxygen concentration, generated on Sigma Plot. The slope of this line represents the reaction order for oxygen concentration within the rate law. One of two oxygen concentrations (0.995 and 0.1 atm) was used for all experiments. The outer solid lines represent a 95% confidence interval.

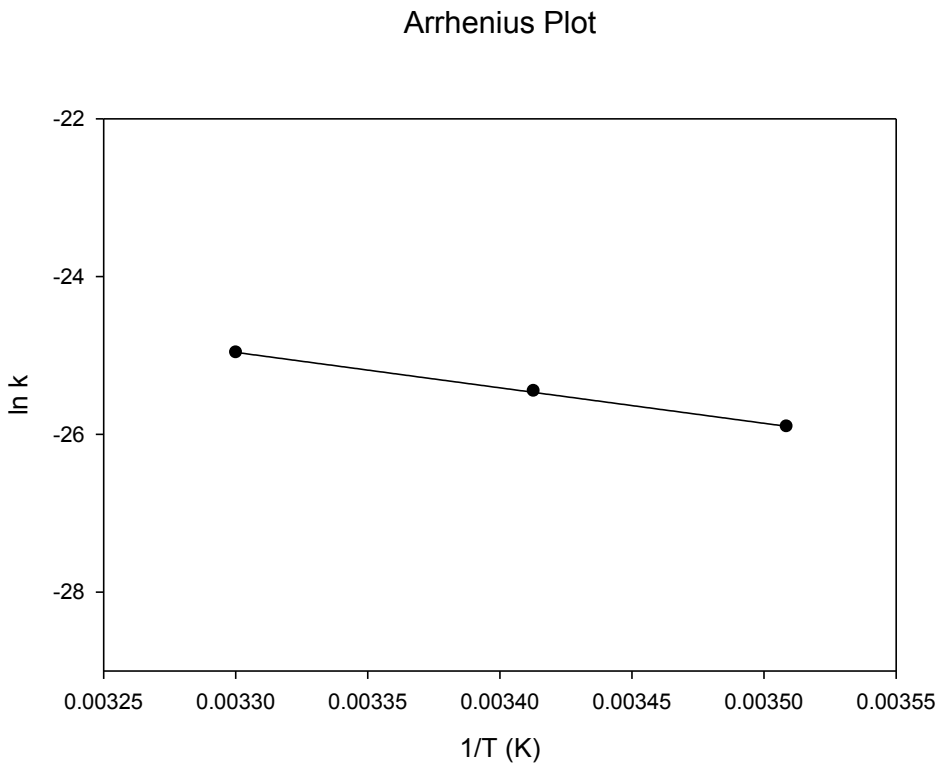

Figure 19. Arrhenius plot. Data from runs with conditions pH: 2.5±0.2 and O_2: 0.995 atm and temperatures of 12, 20, and 30°C. The activation energy (E_a) calculated from this graph is 37.08 kJ/mol. The linear relationship suggests that the E_a for pyrite oxidation in seawater remains consistent across a range of temperatures.

Appendix A

Compiled run data, linear regression coefficients and Arrhenius plot data for experiments that tested the effects of pH, temperature, and dissolved oxygen on the oxidation rate of pyrite in artificial seawater. Each set of conditions was tested multiple times for validity but only select duplicates were chosen to determine the rate law. Ideally 24 samples were taken per experiment. Samples were taken most frequently at the beginning of the experiment because of the concern for a decrease in oxidant availability later in the experiment due to the limitations of the batch reactor design (McKibben and Barnes 1986).

Experiment 2J

Initial pH: 2.05 O_2: 0.995 atm Temperature: 293.5 K

SA V^{-1}: 0.018444

Time (sec)	Sample ID	Dilution Factor (mass)	Vessel Temp (K)	^{56}Fe (mol L^{-1})	Notes
0	Blank	9.222253425	294.5	0	cloudy seawater
180	2J_1	9.348698589	294.5	8.7887E-11	
300	2J_2	9.172619048	294.5	2.7348E-10	2K duplicate run
600	2J_3	9.161932099	294.5	1.5848E-10	
1500	2J_4	9.228012379	293.5	2.125E-10	
2700	2J_5	9.009039436	293.5	3.804E-10	
4200	2J_6	9.082657702	293.5	3.7767E-10	
6300	2J_7	9.132631788	293	3.6158E-10	
9015	2J_8	9.168884035	293	5.7875E-10	sample 15 sec late
12300	2J_9	9.148420425	293.5	8.9346E-10	
14400	2J_10	9.177019855	293	9.1351E-10	
18000	2J_11	9.056267245	292.9	9.3652E-10	
21600	2J_12	9.265427215	292.9	1.0711E-09	
25200	2J_13	9.474725053	293.2	1.2338E-09	
29100	2J_14	9.134640135	293	1.3372E-09	
33300	2J_15	9.519704184	293	1.4918E-09	
37800	2J_16	9.309090909	293	1.4998E-09	
43200	2J_17	9.335344146	293	1.5782E-09	
80040	2J_18	9.186670628	292	2.8915E-09	
86400	2J_19	9.177596701	293	3.5101E-09	
93600	2J_20	8.882583939	293	3.9056E-09	
104700	2J_21	8.968020657	293	4.3312E-09	
115440	2J_22	9.141083744	292.8	5.9606E-09	
159900	2J_23	12.90050661	292.8	6.1791E-09	
172875	2J_24	9.044949346	293	6.2931E-09	

Experiment 2K

Initial pH: 2.05 O_2: 0.995 atm Temperature: 293.5 K

SA V^{-1}: 0.018444

Time (sec)	Sample ID	Dilution Factor (mass)	Vessel Temp (K)	^{56}Fe (mol L^{-1})	Notes
0	Blank	9.314419912	295	0	cloudy seawater
180	2K_1	9.440865076	294	2.92958E-11	
300	2K_2	9.264785535	294	9.11595E-11	
600	2K_3	9.254098586	293.5	1.58482E-10	
1500	2K_4	9.320178866	293.5	2.12503E-10	
2700	2K_5	9.101205923	294	1.26799E-10	
4200	2K_6	9.174824189	294	1.45889E-10	
6300	2K_7	9.224798275	294	1.20526E-10	
9000	2K_8	9.261050522	293	1.92917E-10	
12300	2K_9	9.240586912	292.5	2.97821E-10	
14400	2K_10	9.269186342	292.9	3.04504E-10	
18000	2K_11	9.148433732	293	3.12173E-10	
21600	2K_12	9.357593702	293	3.57045E-10	
25200	2K_13	9.56689154	292.5	4.11259E-10	
29100	2K_14	9.226806622	293	4.45732E-10	
33300	2K_15	9.611870671	292.8	4.97251E-10	
37800	2K_16	9.401257396	293	4.99919E-10	
43200	2K_17	9.427510633	292.8	5.26069E-10	
80040	2K_18	9.278837115	292.8	9.63823E-10	
86400	2K_19	9.269763188	293	1.32623E-09	
93600	2K_20	8.974750426	292.9	1.17003E-09	
104700	2K_21	9.060187144	292.8	1.30188E-09	
115440	2K_22	9.233250231	292.9	1.44372E-09	
159900	2K_23	9.992673101	292.8	1.3202E-09	
172875	2K_24	9.137115833	293	2.05971E-09	

Experiment 2L

Initial pH: 3.03 O_2: 0.995 atm Temperature: 293 K

SA V^{-1}: 0.018444

Time (sec)	Sample ID	Dilution Factor (mass)	Vessel Temp (K)	^{56}Fe (mol L^{-1})	Notes
0	Blank	9.651986945	293	0	
180	2L_1	9.510678298	293	2.9296E-11	
300	2L_2	9.655713754	293	9.116E-11	
620	2L_3	9.496378254	293	1.2848E-10	
1500	2L_4	9.550854294	293	1.425E-10	
2700	2L_5	9.548909467	293	1.868E-10	
4200	2L_6	9.642741732	293.5	1.9589E-10	
6300	2L_7	9.674234088	293.5	2.2353E-10	
9000	2L_8	9.588420721	293.2	2.3292E-10	
11700	2L_9	9.683410625	293	2.9782E-10	
14400	2L_10	9.835196083	293.2	3.045E-10	
18000	2L_11	9.551937497	293.2	3.1217E-10	
21600	2L_12	9.660899688	293.2	3.5705E-10	
25200	2L_13	9.684893222	293	4.1126E-10	
29100	2L_14	9.794783175	292.8	4.4573E-10	
33300	2L_15	9.660713825	293	4.9725E-10	
37800	2L_16	9.625679775	293	5.4992E-10	
43200	2L_17	9.829833281	293	5.8607E-10	
79200	2L_18	9.722913998	293.5	9.6382E-10	
93600	2L_19	9.787161099	293.5	1.17E-09	
108000	2L_20	9.845077292	294	1.3019E-09	
118800	2L_21	9.792561459	294	1.4022E-09	
159588	2L_22	9.740794912	293.5	1.6597E-09	

Experiment 2M

Initial pH: 3.03 O_2: 0.995 atm Temperature: 293.5 K

SA V^{-1}: 0.018444

Time (sec)	Sample ID	Dilution Factor (mass)	Vessel Temp (K)	^{56}Fe (mol L^{-1})	Notes
0	Blank	9.5448228	294	0	1.7g freshly cleaned pyrite
180	2M_1	9.4035141	294	1.8849E-11	0.3g leftover pyrite
300	2M_2	9.5485496	294	1.382E-10	
620	2M_3	9.3892141	294	1.7563E-10	2L duplicate run
1500	2M_4	9.4436901	294	2.1535E-10	
2700	2M_5	9.4417453	293.5	2.534E-10	
4200	2M_6	9.5355776	293.5	2.9447E-10	
6300	2M_7	9.5670699	293.5	3.3345E-10	
9000	2M_8	9.4812565	293.5	3.7288E-10	
11700	2M_9	9.5762464	293.5	4.388E-10	
14400	2M_10	9.7280319	293.2	4.6943E-10	
18000	2M_11	9.4447733	293.2	5.3746E-10	
21600	2M_12	9.5537355	293.2	5.8676E-10	
25200	2M_13	9.5777290	293	6.5839E-10	
29100	2M_14	9.6876190	292.8	7.0257E-10	
33300	2M_15	9.5535496	293	7.9079E-10	
37800	2M_16	9.5185156	293	7.9722E-10	
86400	2M_17	9.7226691	293	1.7006E-09	
93600	2M_18	9.6157498	293	1.7272E-09	run ended early due to pump tubing failure

Experiment 2H

Initial pH: 3.51 O_2: 0.995 atm Temperature: 293.5 K

SA V^{-1}: 0.018444

Time (sec)	Sample ID	Dilution Factor (mass)	Vessel Temp (K)	^{56}Fe (mol L^{-1})	Notes
0	Blank	9.3808150	294	0	pH meter malfunction;
185	2H_1	8.9590557	294	3.87356E-10	used Lyons' meter
360	2H_2	9.2214842	294	4.04356E-10	
600	2H_3	9.2257499	294	4.16356E-10	
1500	2H_4	9.2524272	294	4.57356E-10	
2700	2H_5	9.2240860	293.5	5.92356E-10	
4215	2H_6	9.2589878	293.5	6.38356E-10	
6300	2H_7	9.3142714	293.5	7.45356E-10	
9000	2H_8	9.3185564	293.5	9.49356E-10	
12330	2H_9	9.2860284	293.5	1.07236E-09	
14400	2H_10	9.1793519	293.2	1.14236E-09	
18000	2H_11	9.3256672	293.2	1.37236E-09	
21600	2H_12	9.2935249	293.2	1.56236E-09	
25200	2H_13	9.2606464	293	1.67236E-09	
29100	2H_14	9.2547175	292.8	1.80236E-09	
33300	2H_15	9.3209498	293	1.94236E-09	
37800	2H_16	9.2773066	293	2.22236E-09	
43200	2H_17	9.3865300	293	2.46236E-09	
79200	2H_18	9.3918677	293	4.30236E-09	
86400	2H_19	9.2781067	293	4.84236E-09	
96660	2H_20	9.3029787	293	5.28236E-09	
108000	2H_21	9.5217268	292.8	5.69236E-09	
118845	2H_22	9.3634655	292.8	6.36236E-09	
129600	2H_23	9.0988577	293	6.55236E-09	
163880	2H_24	9.1901217	293	7.53236E-09	

Experiment 2I

Initial pH: 3.52 O_2: 0.995 atm Temperature: 293.5 K

SA V^{-1}: 0.018444

Time (sec)	Sample ID	Dilution Factor (mass)	Vessel Temp (K)	^{56}Fe (mol L)	Notes
0	Blank	9.4338065	294	0	pH meter malfunction;
185	2I_1	9.5120471	294	3.10914E-10	used Lyons' meter
360	2I_2	9.2744757	294	3.27914E-10	
600	2I_3	9.2787413	294	3.39914E-10	2H duplicate run
1500	2I_4	9.3054186	294	3.80914E-10	
2700	2I_5	9.4270775	293.5	5.15914E-10	
4215	2I_6	9.3119792	293.5	5.61914E-10	
6300	2I_7	9.3672629	293.5	6.68914E-10	
9000	2I_8	9.3715478	293.5	8.72914E-10	
12330	2I_9	9.3390198	293.5	9.95914E-10	
14400	2I_10	9.2323433	293.2	1.06591E-09	
18000	2I_11	9.3786586	293.2	1.29591E-09	
21600	2I_12	9.3465164	293.2	1.48591E-09	
25200	2I_13	9.3136379	293	1.59591E-09	
29100	2I_14	9.3077089	292.8	1.72591E-09	
33300	2I_15	9.3739412	293	1.86591E-09	
37800	2I_16	9.3302980	293	2.14591E-09	
43200	2I_17	9.4395224	293	2.38591E-09	
79200	2I_18	9.3448592	293	4.22591E-09	
86400	2I_19	9.3310981	293	4.76591E-09	
96660	2I_20	9.3559702	293	5.20591E-09	
108000	2I_21	9.5747182	292.8	5.61591E-09	
118845	2I_22	9.4164570	292.8	6.28591E-09	
129600	2I_23	9.1518491	293.2	6.47591E-09	
163880	2I_24	9.2431131	293.5	7.45591E-09	

Experiment 2A

Initial pH: 4.04 O_2: 0.995 atm Temperature: 293.5 K

SA V^{-1}: 0.018444

Time (sec)	Sample ID	Dilution Factor (mass)	Vessel Temp (K)	^{56}Fe (mol L^{-1})	Notes
0	Blank	9.5283316	293	0	
180	2A_1	9.3608567	293	5.78193E-11	
300	2A_2	9.3477940	293.5	6.14803E-11	
620	2A_3	9.3153967	294	9.30843E-11	
1500	2A_4	9.3025371	294	7.80683E-11	
2700	2A_5	9.3844790	293.5	1.24359E-10	
4200	2A_6	9.3567634	293.5	1.03109E-10	
6300	2A_7	9.3865857	293.5	1.36529E-10	
9000	2A_8	9.4338133	293.5	1.53859E-10	
11700	2A_9	9.3447223	293.5	1.65252E-10	
14400	2A_10	9.3274031	293.2	1.87289E-10	
18000	2A_11	9.3787017	293.2	2.32509E-10	
21600	2A_12	9.4315851	293.2	2.85379E-10	
25200	2A_13	9.3519759	293	3.04769E-10	
29100	2A_14	9.3786982	292.8	7.35009E-10	
33300	2A_15	9.4868784	293	8.03609E-10	
37800	2A_16	9.4088485	293	7.62349E-10	
42080	2A_17	9.3732505	293	7.64209E-10	
86400	2A_18	9.4127609	293	8.24359E-10	
93600	2A_19	9.5320323	293	8.05169E-10	
97450	2A_20	9.3763212	293	9.23329E-10	
108000	2A_21	9.4149985	293.8	9.70079E-10	
115200	2A_22	9.3546706	292.8	1.32192E-09	
118800	2A_23	9.4360739	293.2	1.36582E-09	
187200	2A_24	9.3444007	293	1.35642E-09	

Experiment 2B

Initial pH: 4.01 O_2: 0.995 atm Temperature: 293.5 K

SA V^{-1}: 0.018444

Time (sec)	Sample ID	Dilution Factor (mass)	Vessel Temp (K)	^{56}Fe (mol L^{-1})	Notes
0	Blank	9.6009785	294	0	~200mL of water lost
180	2B_1	9.4481956	294	5.7091E-11	at beginning of run
300	2B_2	9.4406795	294	6.0661E-11	
620	2B_3	9.4531631	294	9.2265E-11	2A duplicate run
1500	2B_4	9.5600898	294	7.7249E-11	
2700	2B_5	9.4512935	293.5	1.2354E-10	
4200	2B_6	9.5517593	293.5	1.0229E-10	
6300	2B_7	9.5783599	293.5	1.3571E-10	
9000	2B_8	9.5172144	293.5	1.5304E-10	
11700	2B_9	9.5095814	293.5	1.7416E-10	
14400	2B_10	9.5451187	293.2	1.8647E-10	
18000	2B_11	9.5935233	293.2	2.3169E-10	
21600	2B_12	9.6073501	293.2	2.8456E-10	
25200	2B_13	9.5767195	293	3.0395E-10	
29100	2B_14	9.5993136	292.8	7.3419E-10	
33300	2B_15	9.67899852	293	8.0279E-10	
37800	2B_16	9.5940243	293	7.6153E-10	
42080	2B_17	9.5738999	293	7.6339E-10	
86400	2B_18	9.6327453	293	8.2354E-10	
93600	2B_19	9.5363576	293	8.0435E-10	
97450	2B_20	9.6530986	293	9.3251E-10	
108000	2B_21	9.5558938	292.8	9.6926E-10	
115200	2B_22	9.6939362	292.8	1.3211E-09	
118800	2B_23	9.7607576	293.2	1.305E-09	
187200	2B_24	9.6676806	293	1.3056E-09	

Experiment 1I

Initial pH: 4.54 O_2: 0.995 atm Temperature: 292.5 K

SA V^{-1}: 0.018444

Time (sec)	Sample ID	Dilution Factor (mass)	Vessel Temp (K)	^{56}Fe (mol L^{-1})	Notes
0	Blank	9.679362807	292	0	
180	1I_1	9.257603459	292	8.6975E-11	
300	1I_2	9.520031996	292.2	8.3319E-11	
420	1I_3	9.524297638	292.5	9.2731E-11	
660	1I_4	9.550974933	292.5	1.7672E-10	
900	1I_5	9.522633798	292.5	1.9027E-10	
1280	1I_6	9.55753555	292.5	1.8971E-10	
1800	1I_7	9.612819198	292.5	2.2409E-10	
2420	1I_8	9.617104119	292.2	2.5429E-10	
5400	1I_9	9.584576174	292	2.9858E-10	
6300	1I_10	9.477899615	292	3.1092E-10	
8340	1I_11	9.624214932	292	3.7403E-10	
9000	1I_12	9.5920727	292.5	3.4531E-10	
11420	1I_13	9.559194195	293	4.1836E-10	
13260	1I_14	9.553265211	293	4.7795E-10	
14415	1I_15	9.619497561	293	4.8589E-10	
16260	1I_16	9.575854317	293	5.2824E-10	
17700	1I_17	9.685077712	292.5	5.5295E-10	
19800	1I_18	9.690415503	292.5	5.9716E-10	
21675	1I_19	9.576654462	293	6.4974E-10	
23400	1I_20	9.601526497	293	6.8497E-10	
25200	1I_21	9.820274518	292.8	6.9239E-10	
27150	1I_22	9.662013294	292.5	7.1843E-10	

Experiment 1J

Initial pH: 4.54 P_{O2} : 0.995 atm Temperature: 293.5 K

SA V^{-1}: 0.018444

Time (sec)	Sample ID	Dilution Factor (mass)	Vessel Temp (K)	^{56}Fe (mol L^{-1})	Notes
0	Blank	9.1184575	294	0	oxygen off until
180	1J_1	9.3091508	294	8.8378E-11	4 min into run
300	1J_2	9.1498200	294	8.0326E-11	
420	1J_3	9.2143642	294	8.4926E-11	
660	1J_4	9.4500626	294	1.8435E-10	
900	1J_5	9.1076877	293.5	1.7959E-10	
1280	1J_6	9.1807630	293.5	1.4971E-10	
1800	1J_7	9.1540857	293.5	2.1292E-10	
2420	1J_8	9.2426072	293.5	2.1949E-10	
3000	1J_9	9.1889822	293.5	2.5863E-10	
3900	1J_10	9.0271935	293.2	2.7014E-10	
5400	1J_11	9.2056424	293.2	2.9858E-10	
6300	1J_12	9.2468922	293.2	2.9092E-10	
8340	1J_13	9.3148658	293	3.3646E-10	
9000	1J_14	9.2492856	292.8	3.5931E-10	
10260	1J_15	9.1830533	293	3.6836E-10	
13260	1J_16	8.8873915	293	4.4795E-10	
14415	1J_17	9.2064425	293	4.8589E-10	
16260	1J_18	9.1873236	293	5.1924E-10	
17700	1J_19	9.2218607	293	5.6595E-10	
19800	1J_20	9.2918013	293	5.9716E-10	
21675	1J_21	9.3202035	292.8	6.0774E-10	
23400	1J_22	9.1524218	292.8	6.8497E-10	
25200	1J_23	9.2540030	293	6.9239E-10	
27150	1J_24	9.2313145	293	6.8243E-10	

Experiment X

Initial pH: 5.05 O_2: 0.995 atm Temperature: 293.5 K

SA V^{-1}: 0.018444

Time (sec)	Sample ID	Dilution Factor (mass)	Vessel Temp (K)	^{56}Fe (mol L^{-1})	Notes
0	Blank	9.242943224	294	0	note pH and
180	X_1	9.08721402	294	8.44512E-11	short run time
300	X_2	9.165589369	294	7.63992E-11	
420	X_3	9.100120677	294	8.09992E-11	
660	X_4	9.17867809	294	2.80423E-10	
900	X_5	9.237881089	293.5	3.75663E-10	
1280	X_6	9.109150955	293.5	1.45783E-10	
1800	X_7	9.200531812	293.5	2.08993E-10	
2420	X_8	9.129307938	293.5	2.15563E-10	
3000	X_9	9.25826718	293.5	2.54703E-10	
3900	X_10	9.298113056	294	2.66213E-10	
5400	X_11	9.305593648	294	2.94653E-10	
6300	X_12	9.242634905	293.5	2.86993E-10	
8340	X_13	9.315927576	293	3.72533E-10	
9000	X_14	9.278684823	293	3.55383E-10	
10260	X_15	9.248950885	293	3.64433E-10	
13260	X_16	9.345048686	293	4.44023E-10	
14415	X_17	9.519979124	293	4.68963E-10	
18260	X_18	9.36598176	293	6.15313E-10	
22700	X_19	9.269140792	293	5.77023E-10	
23800	X_20	9.344811253	293	5.93233E-10	
26675	X_21	9.265647462	293.5	6.03813E-10	
31400	X_22	9.464543069	293.8	6.81043E-10	
35200	X_23	9.325377956	294	6.88463E-10	
39360	X_24	9.339731778	294	6.78503E-10	

Experiment 3A

Initial pH: 2.47 O_2: 0.10 atm Temperature: 294 K

SA V^{-1}: 0.018444

Time (sec)	Sample ID	Dilution Factor (mass)	Vessel Temp (K)	^{56}Fe (mol L^{-1})	Notes
0	Blank	9.457481	295	0	dissolved O2 measured
180	3A_1	9.197839	294.8	7.4742E-11	at 1.84 mg L^{-1}
370	3A_2	9.258818	294.5	1.6679E-10	where
600	3A_3	9.376825	293.4	1.5011E-10	1.84 mg L^{-1} =
1500	3A_4	9.336844	294.1	2.1651E-10	5.6372E-05 mol kg^{-1}
2700	3A_5	9.271411	294.5	2.6381E-10	
4200	3A_6	9.293344	294	3.4464E-10	
6300	3A_7	9.313796	293.8	3.971E-10	
9000	3A_8	9.317947	293.8	6.3955E-10	
11880	3A_9	9.280451	293.8	4.6448E-10	
14400	3A_10	9.316189	293.8	4.9997E-10	
18000	3A_11	9.352402	293.8	5.4914E-10	
21600	3A_12	9.303646	293.6	5.4477E-10	
29130	3A_13	9.340450	294	6.7287E-10	
66100	3A_14	9.336486	293.8	1.0337E-09	
70200	3A_15	9.345174	294	1.0891E-09	
77280	3A_16	9.322124	293.8	1.2691E-09	
90900	3A_17	9.458080	293.8	1.2651E-09	
105100	3A_18	9.468114	293.8	1.3765E-09	
147600	3A_19	9.818740	293.6	1.8818E-09	
157020	3A_20	9.265596	294	1.8173E-09	
167820	3A_21	9.310989	293.8	1.8912E-09	
174900	3A_22	9.325595	293.8	1.9693E-09	
183600	3A_23	9.281420	293.6	2.0082E-09	
191200	3A_24	9.372684	293.5	2.1773E-09	

Experiment 3B

Initial pH: 2.47 O_2: 0.10 atm Temperature: 294 K

SA V^{-1}: 0.018444

Time (sec)	Sample ID	Dilution Factor (mass)	Vessel Temp (K)	^{56}Fe (mol L^{-1})	Notes
0	Blank	8.3775404	294	0	3A duplicate run
180	3B_1	9.2973234	293.8	7.0704E-11	
370	3B_2	9.3418164	294	9.7426E-11	
600	3B_3	9.4078228	293.8	9.9022E-11	
1500	3B_4	9.4472055	294	1.3952E-10	
2700	3B_5	9.4185268	294	1.3748E-10	
4200	3B_6	9.5107012	294.2	1.8097E-10	
6300	3B_7	9.4523809	294	1.9065E-10	
9000	3B_8	9.3767744	294	2.6493E-10	
11880	3B_9	9.4408517	293.8	2.5104E-10	
14400	3B_10	9.3515887	293.8	7.36975E-10	
18000	3B_11	9.5366094	293.8	6.94006E-10	
21600	3B_12	9.4527613	293.8	3.3522E-10	
29130	3B_13	9.4686208	293.6	4.07E-10	
66100	3B_14	9.3789629	294	7.4755E-10	
70200	3B_15	9.4637995	294	7.9256E-10	
77280	3B_16	9.3714257	294	8.364E-10	
90900	3B_17	9.5219536	294	9.7616E-10	
105100	3B_18	9.4180724	293.8	1.1082E-09	
147600	3B_19	9.4324111	293.8	1.4642E-09	
157020	3B_20	9.3010501	293.8	1.6875E-09	
167820	3B_21	9.4678627	294	1.4637E-09	
174900	3B_22	9.5460286	294	1.6466E-09	

Experiment 2W

Initial pH: 2.55 O_2: 0.10 atm Temperature: 293.5 K

SA V^{-1}: 0.018444

Time (sec)	Sample ID	Dilution Factor (mass)	Vessel Temp (K)	^{56}Fe (mol L^{-1})	Notes
0	Blank	9.0978900	294	0	in vessel ~3min
180	2W_1	8.9565813	294	3.2802E-11	before oxygen flow;
300	2W_2	9.1016168	294	6.0661E-11	timer started
600	2W_3	8.9422813	294	9.2265E-11	upon O2 flow.
1500	2W_4	8.9967573	294	7.7249E-11	oxygen measured at
2700	2W_5	8.9948125	293.5	1.2354E-10	1.77 mg L^{-1}
4200	2W_6	9.0886448	293.5	1.0229E-10	where
6300	2W_7	9.1201371	293.5	1.3571E-10	1.77 mg L^{-1} =
9000	2W_8	9.0343238	293.5	1.5304E-10	5.422E-05 mol kg^{-1}
11700	2W_9	9.1293137	293.5	1.8529E-10	
14760	2W_10	9.2810991	293.2	1.8647E-10	
18000	2W_11	8.9978405	293.2	2.3169E-10	
21600	2W_12	9.1068027	293.2	2.8456E-10	
25500	2W_13	9.1307963	293	3.0395E-10	
88800	2W_14	9.2406862	292.8	7.3419E-10	
92400	2W_15	9.1066169	293	8.0279E-10	
96000	2W_16	9.0715828	293	7.6153E-10	
99600	2W_17	9.2757363	293	7.6339E-10	
103200	2W_18	9.1688170	293	8.2354E-10	
106800	2W_19	9.2330641	293	8.0435E-10	
114000	2W_20	9.2909803	293	9.3251E-10	
126000	2W_21	9.2384645	292.8	9.6926E-10	
180000	2W_22	9.1866980	292.8	9.4101E-10	
183600	2W_23	9.2155999	293.2	1.4819E-09	
187200	2W_24	9.2013146	293	1.5368E-09	

Experiment 2X

Initial pH: 2.55 O_2: 0.10 atm Temperature: 294 K

SA V^{-1}: 0.018444

Time (sec)	Sample ID	Dilution Factor (mass)	Vessel Temp (K)	^{56}Fe (mol L^{-1})	Notes
0	Blank	9.156427015	295	0	pump tubing installed
180	2X_1	9.044400978	295	6.4636E-11	backwards;
300	2X_2	9.13032851	295	6.543E-11	timer started once O2
600	2X_3	9.197213501	294.2	6.8759E-11	flowed
1500	2X_4	9.218250049	294.2	1.3453E-10	
2700	2X_5	9.221275753	294	1.0155E-10	
4200	2X_6	9.098385019	294	1.1942E-10	
6300	2X_7	9.177782202	294	1.6352E-10	
9000	2X_8	9.22814668	294.2	1.8127E-10	
11700	2X_9	9.054920134	294	2.0252E-10	
14760	2X_10	9.386752988	294	2.2608E-10	
18000	2X_11	9.920003975	294.2	2.9949E-10	
21600	2X_12	9.186906646	294.2	3.1569E-10	
25500	2X_13	9.325292833	294	3.4132E-10	
88800	2X_14	9.22292804	293.5	8.6259E-10	
92400	2X_15	9.139336116	293.8	9.3938E-10	
96000	2X_16	9.365482234	294	9.5005E-10	
99600	2X_17	9.327205882	294	1.0004E-09	experiment ended early;
103200	2X_18	9.161835041	293.5	9.6384E-10	due to pump tubing rip

Experiment 3H

Initial pH: 2.95 O_2: 0.995 atm Temperature: 285 K

SA V^{-1}: 0.018444

Time (sec)	Sample ID	Dilution Factor (mass)	Vessel Temp (K)	^{56}Fe (mol L^{-1})	Notes
0	Blank	9.853371306	286	0	low temp run
180	3H_1	9.592215746	285.7	7.626E-11	
300	3H_2	9.577063767	286	2.6887E-11	
600	3H_3	9.491124841	285.9	2.0374E-11	
1500	3H_4	9.533058257	285.7	4.9774E-11	
2700	3H_5	9.500925114	285.4	8.0553E-11	
4200	3H_6	9.532434295	285.2	1.0451E-10	
6346	3H_7	9.573616601	285.2	1.1798E-10	
9000	3H_8	9.29988466	285.2	1.4278E-10	
11700	3H_9	9.585537919	285	1.902E-10	
14400	3H_10	10.08082998	285	2.3577E-10	
17800	3H_11	9.350811486	285	2.346E-10	
21600	3H_12	9.377321793	285	2.6515E-10	
77400	3H_13	9.856743257	285	5.9588E-10	
82800	3H_14	9.333461761	285	6.0035E-10	
88200	3H_15	9.629084806	284.9	6.5471E-10	
93600	3H_16	9.93095723	285	6.9284E-10	
99000	3H_17	9.52506339	285	6.9318E-10	
104400	3H_18	9.639865333	285	7.0827E-10	
172800	3H_19	9.376550928	285	9.2533E-10	
176400	3H_20	9.410736822	284.8	1.1041E-09	
180000	3H_21	9.543207455	284.9	1.1403E-09	
241380	3H_22	9.962671132	285	1.1475E-09	ended at 67 hours

Experiment 3I

Initial pH: 2.98 O_2: 0.995 atm Temperature: 303 K

SA V^{-1}: 0.018444

Time (sec)	Sample ID	Dilution Factor (mass)	Vessel Temp (K)	^{56}Fe (mol L^{-1})	Notes
0	Blank	9.563378127	299	0	high temp run
185	3I_1	9.141618779	299	3.9445E-12	
360	3I_2	9.404047316	299	1.3417E-10	
600	3I_3	9.408312958	299.5	5.4562E-11	
1510	3I_4	9.434990253	301	2.0822E-10	
2700	3I_5	9.406649118	303.8	2.1279E-10	
4650	3I_6	9.44155087	303	3.3407E-10	
6350	3I_7	9.496834518	302.5	4.0803E-10	
9000	3I_8	9.501119439	302.8	5.4717E-10	
11700	3I_9	9.468591494	302.6	6.128E-10	
14400	3I_10	9.361914935	302.8	8.1133E-10	
18000	3I_11	9.508230252	303	9.8309E-10	
24060	3I_12	9.47608802	302.6	1.2573E-09	
27000	3I_13	9.443209515	302.8	1.6997E-09	
78500	3I_14	9.437280531	302.5	4.6637E-09	
85300	3I_15	9.503512881	302.5	7.1684E-09	
89000	3I_16	9.459869637	302.5	3.8643E-09	
92100	3I_17	9.569093032	302.6	6.1857E-09	
96200	3I_18	9.574430823	302.6	5.1264E-09	
99800	3I_19	9.460669782	302.4	4.5088E-09	
103500	3I_20	9.485541817	302.5	5.5905E-09	
120000	3I_21	9.704289838	302.5	7.6699E-09	
140000	3I_22	9.546028614	302.5	8.508E-09	ended at 39 hours

Appendix B

All run data as iron concentration vs. time scatter plots generated on the computer graphing software SigmaPlot, version 11. An equation for the quadratic best fit curve was extracted through SigmaPlot. The first derivative of the equation evaluated at zero yielded the log(rate). The two log(rate) plots and the Arrhenius plot are provided in the Figures 17-19.

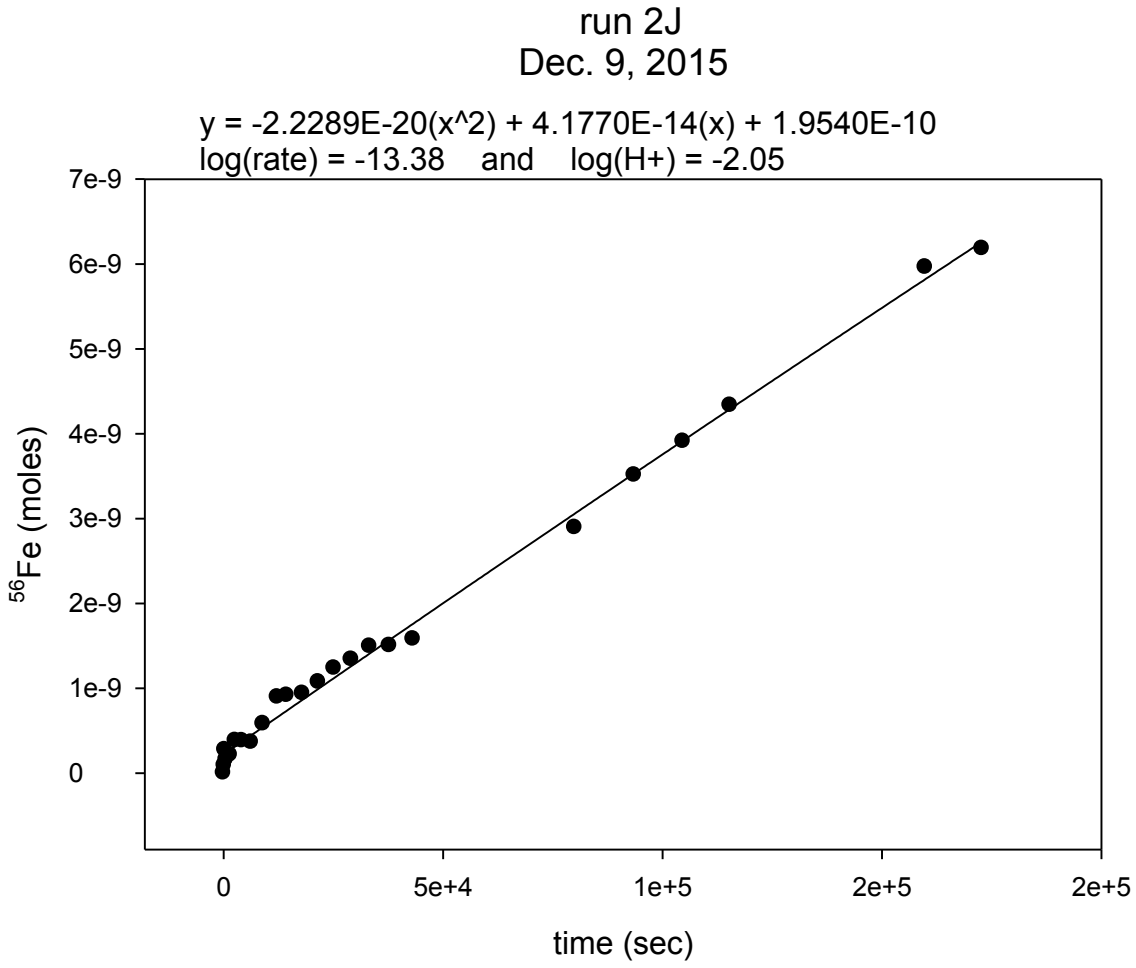

pH = 2.05 P_{O2} = 0.995 atm Temp = 293.5 K SA V^{-1} = 0.018444

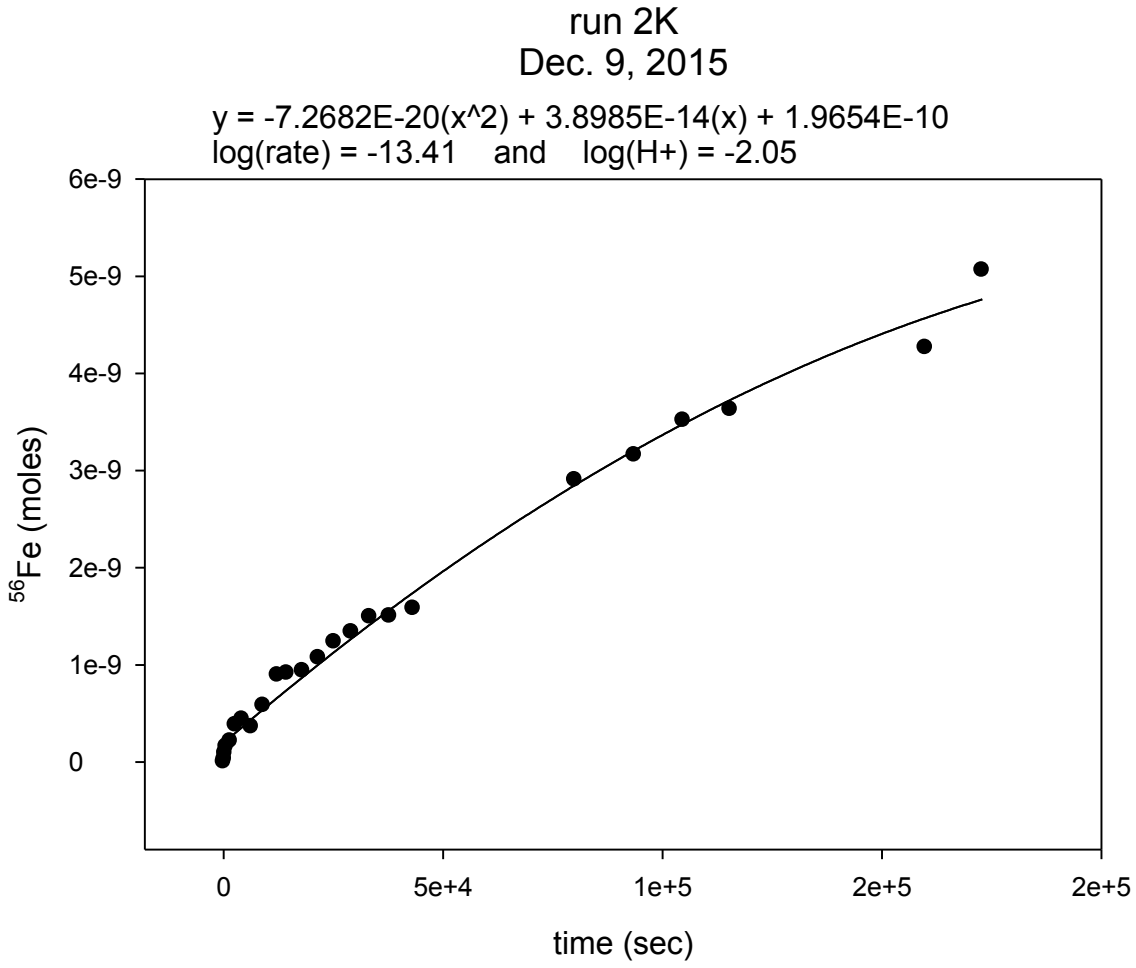

pH = 2.05 P_{O2} = 0.995 atm Temp = 293.5 K SA V^{-1} = 0.018444

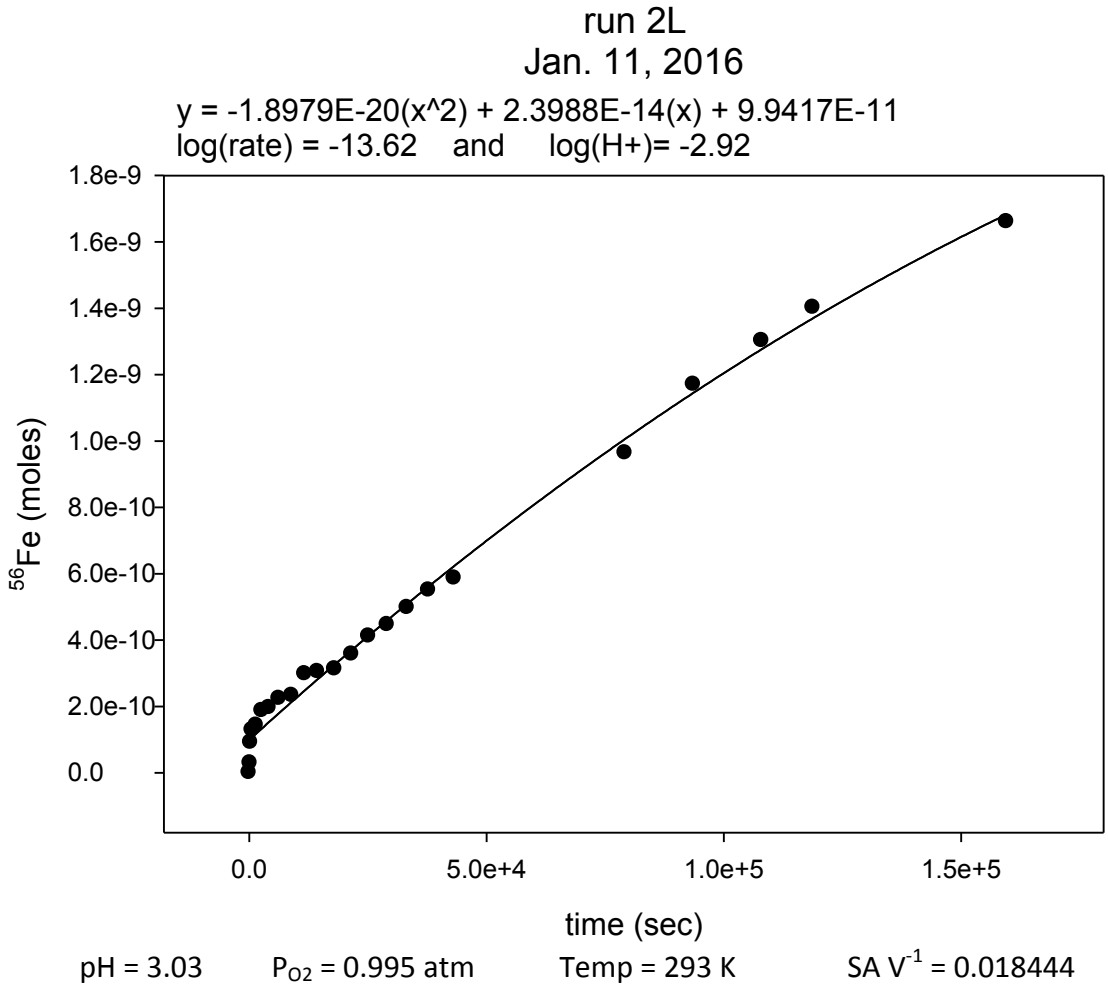
run 2L
Jan. 11, 2016
y = -1.8979E-20(x^2) + 2.3988E-14(x) + 9.9417E-11
log(rate) = -13.62 and log(H+)= -2.92
1.8e-9
1.6e-9
1.4e-9
1.2e-9
1.0e-9
8.0e-10
6.0e-10
4.0e-10
2.0e-10
0.0
56Fe (moles)
0.0
5.0e+4
1.0e+5
1.5e+5
time (sec)
pH = 3.03
PO2 = 0.995 atm
Temp = 293 K
SA V-1 = 0.018444

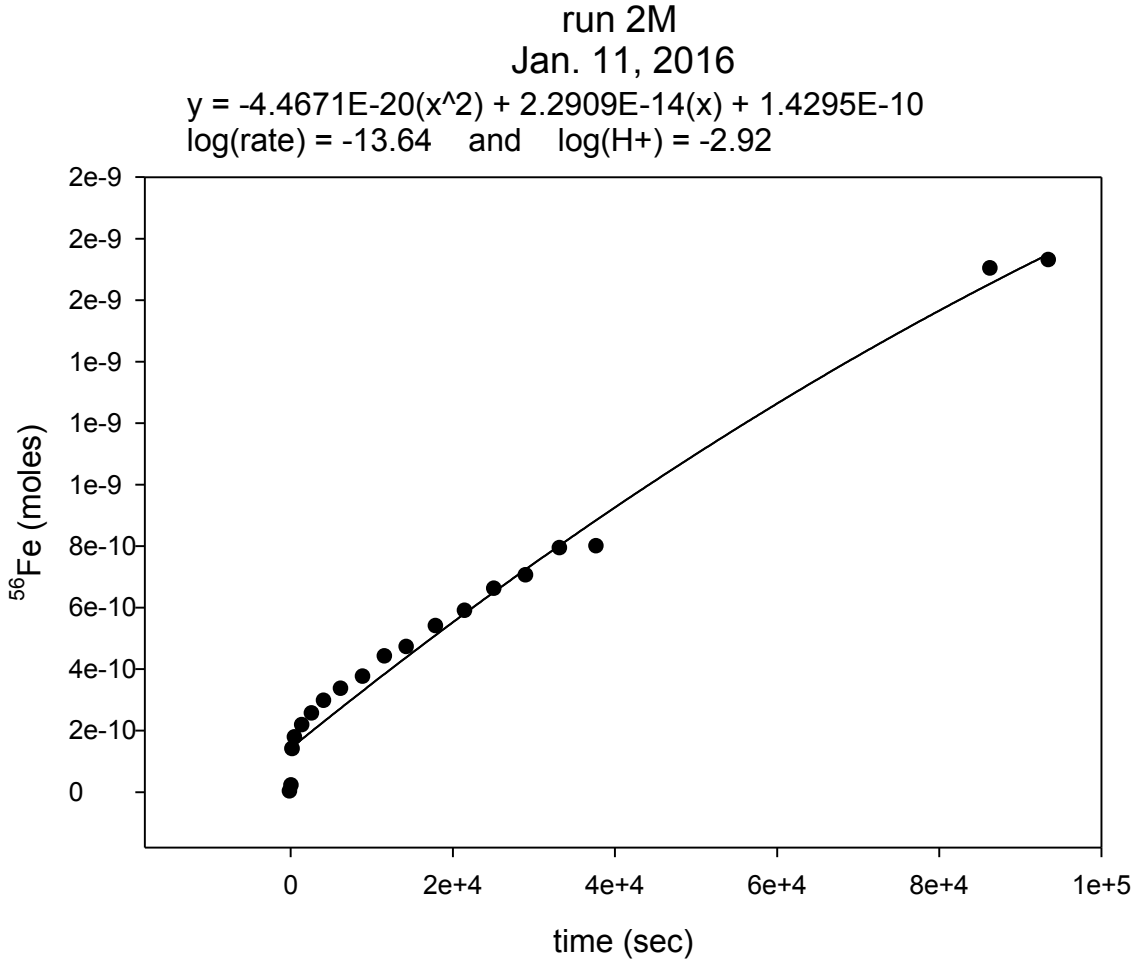

pH = 3.03 P_{O2} = 0.995 atm Temp = 293.5 K SA V^{-1} = 0.018444

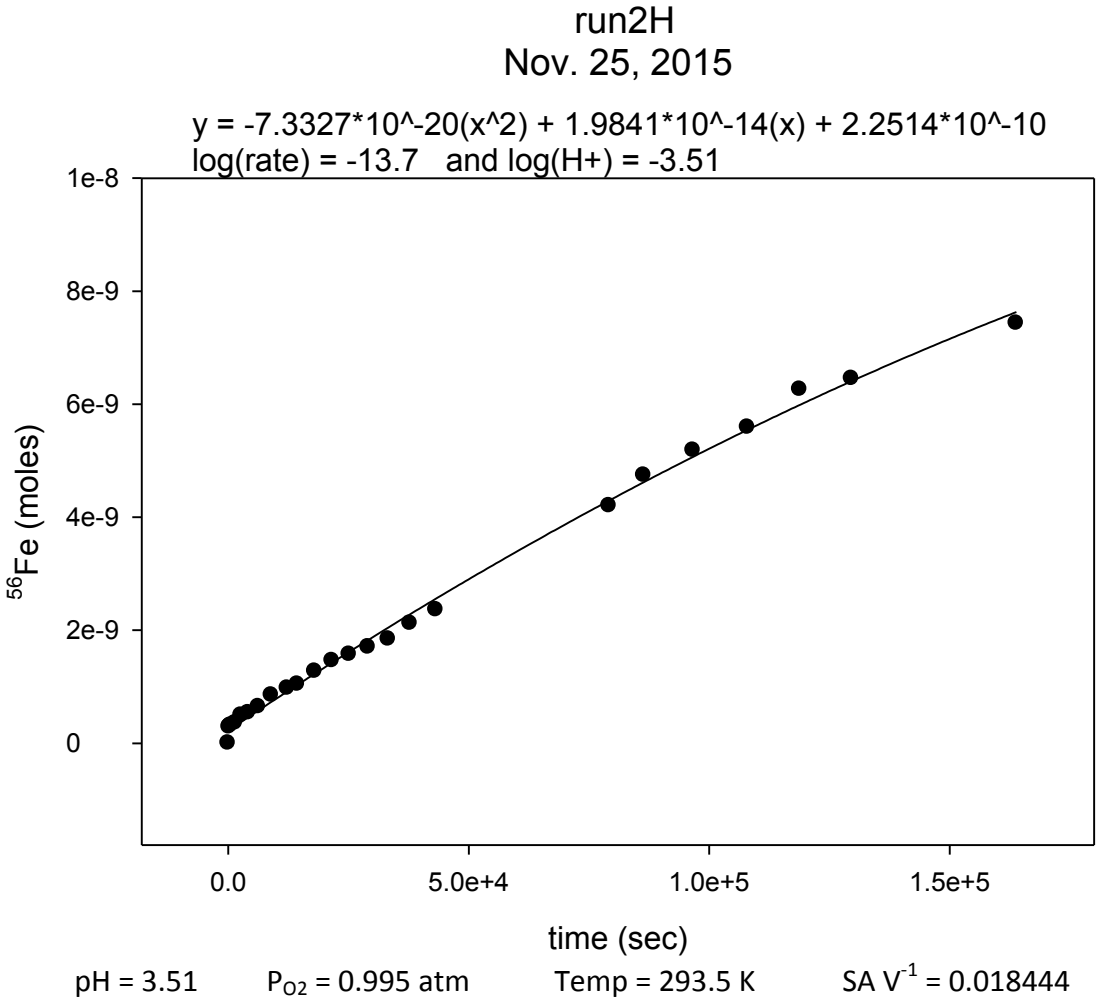
run2H
Nov. 25, 2015
y = -7.3327*10^-20(x^2) + 1.9841*10^-14(x) + 2.2514*10^-10
log(rate) = -13.7 and log(H+) = -3.51
1e-8
8e-9
6e-9
4e-9
2e-9
0
56Fe (moles)
0.0
5.0e+4
1.0e+5
1.5e+5
time (sec)
pH = 3.51
PO2 = 0.995 atm
Temp = 293.5 K
SA V-1 = 0.018444

run 2l
Nov. 25, 2015

y = -6.0611*10^-20(x^2) + 2.0045*10^-14(x) + 2.4947*10^-10
log(rate) = -13.7 and log(H+) = -3.52

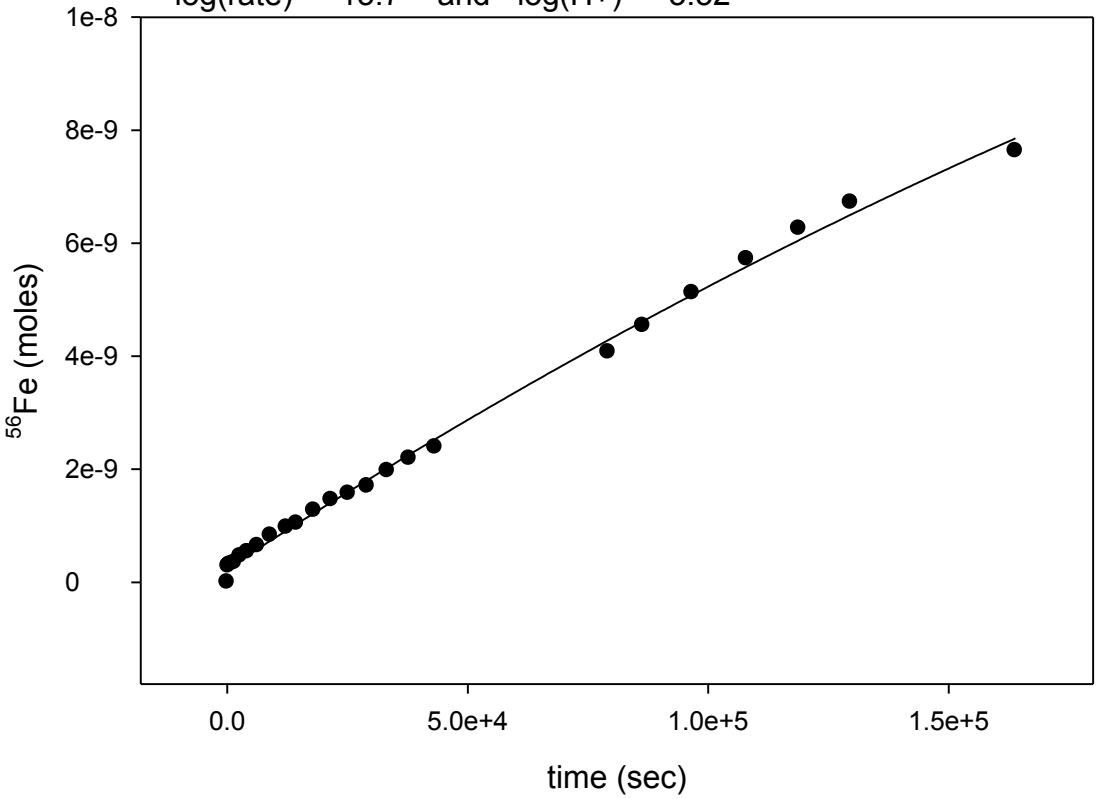

pH = 3.52 P_{O2} = 0.995 atm Temp = 293.5 K SA V^{-1} = 0.018444

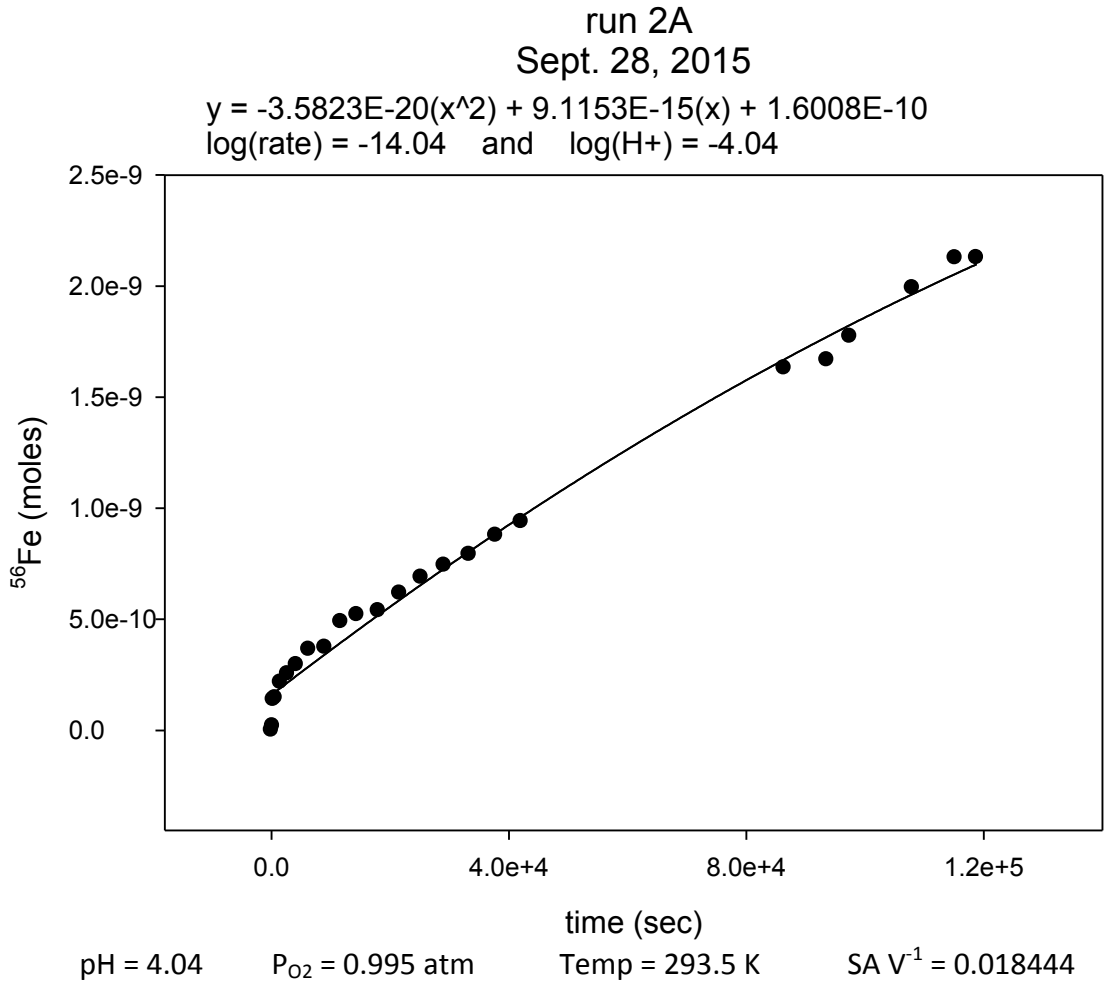
run 2A
Sept. 28, 2015
y = -3.5823E-20(x^2) + 9.1153E-15(x) + 1.6008E-10
log(rate) = -14.04 and log(H+) = -4.04
2.5e-9
2.0e-9
1.5e-9
1.0e-9
5.0e-10
0.0
56Fe (moles)
0.0
4.0e+4
8.0e+4
1.2e+5
time (sec)
pH = 4.04
PO2 = 0.995 atm
Temp = 293.5 K
SA V-1 = 0.018444

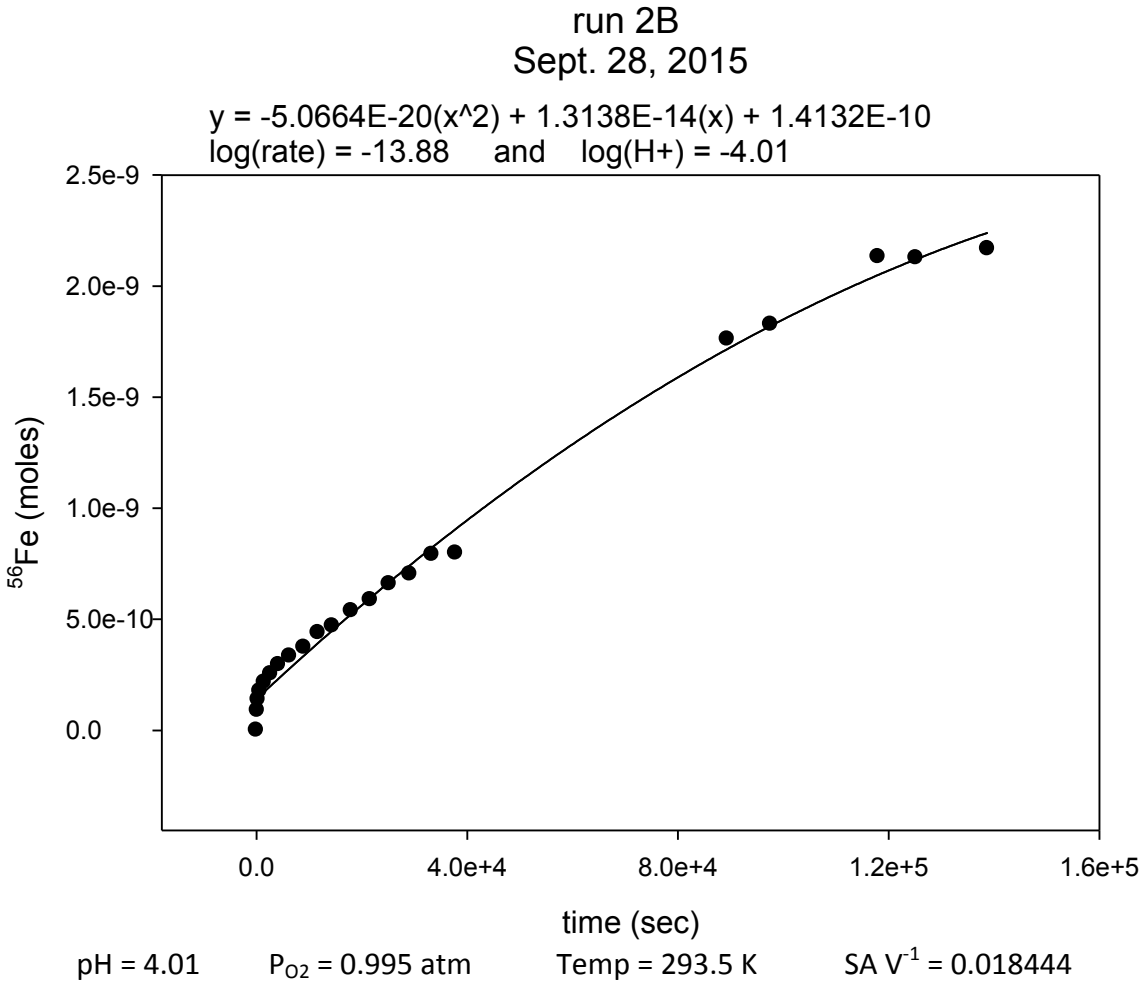
run 2B
Sept. 28, 2015
y = -5.0664E-20(x^2) + 1.3138E-14(x) + 1.4132E-10
log(rate) = -13.88 and log(H+) = -4.01
2.5e-9
2.0e-9
1.5e-9
1.0e-9
5.0e-10
0.0
56Fe (moles)
0.0
4.0e+4
8.0e+4
1.2e+5
1.6e+5
time (sec)
pH = 4.01
PO2 = 0.995 atm
Temp = 293.5 K
SA V-1 = 0.018444

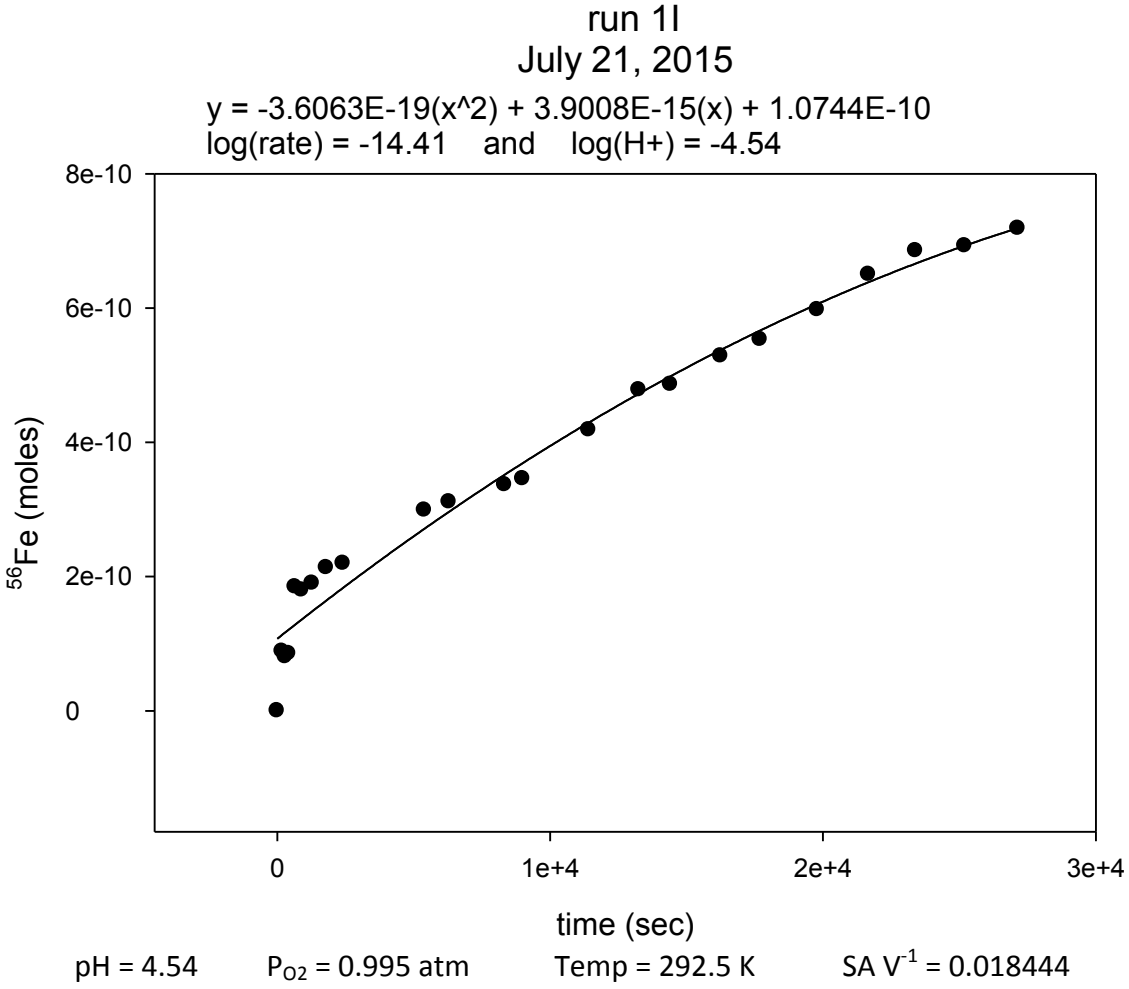
run 1I
July 21, 2015
y = -3.6063E-19(x^2) + 3.9008E-15(x) + 1.0744E-10
log(rate) = -14.41 and log(H+) = -4.54
8e-10
6e-10
4e-10
2e-10
0
56Fe (moles)
0
1e+4
2e+4
3e+4
time (sec)
pH = 4.54
PO2 = 0.995 atm
Temp = 292.5 K
SA V-1 = 0.018444

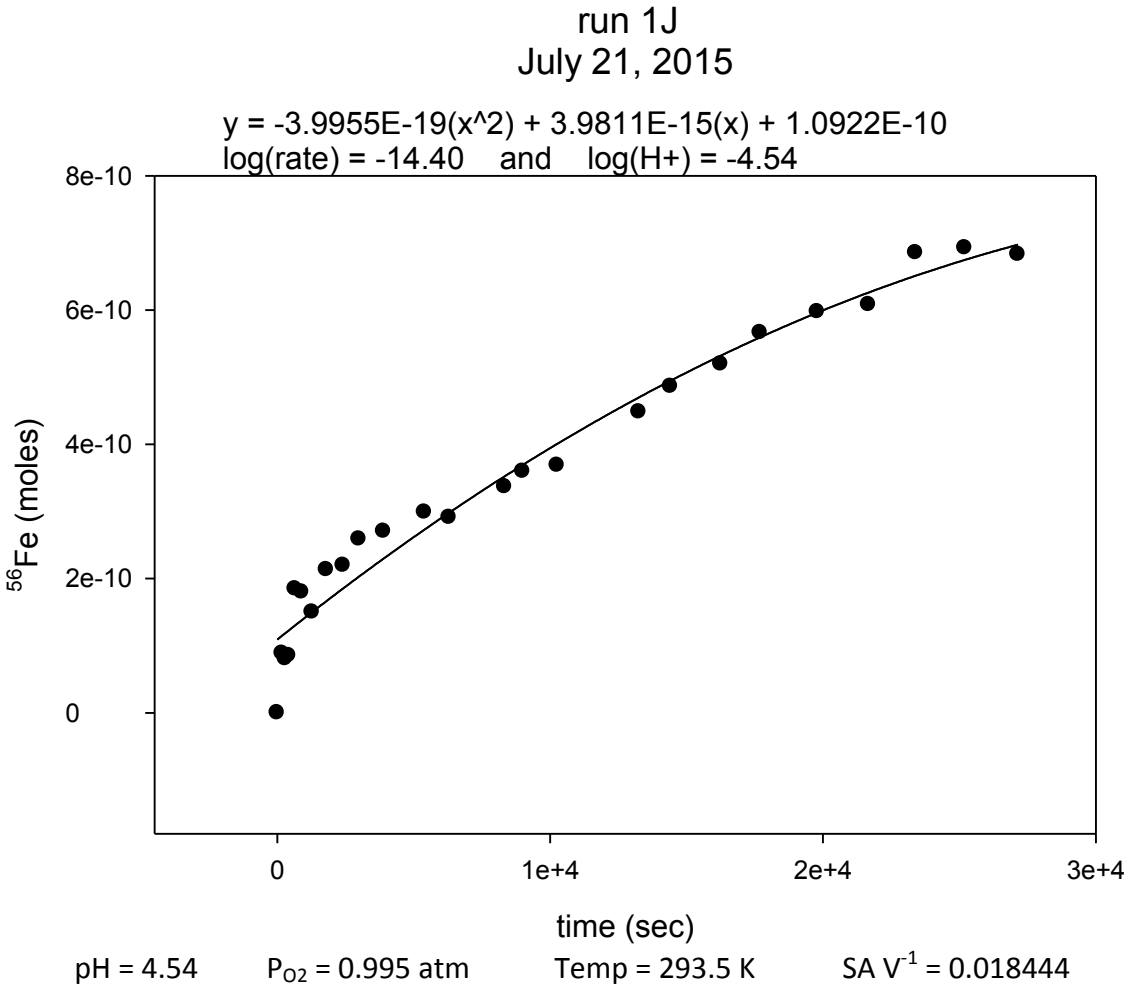
run 1J
July 21, 2015
y = -3.9955E-19(x^2) + 3.9811E-15(x) + 1.0922E-10
log(rate) = -14.40 and log(H+) = -4.54
8e-10
6e-10
4e-10
2e-10
0
56Fe (moles)
0
1e+4
2e+4
3e+4
time (sec)
pH = 4.54
PO2 = 0.995 atm
Temp = 293.5 K
SA V-1 = 0.018444

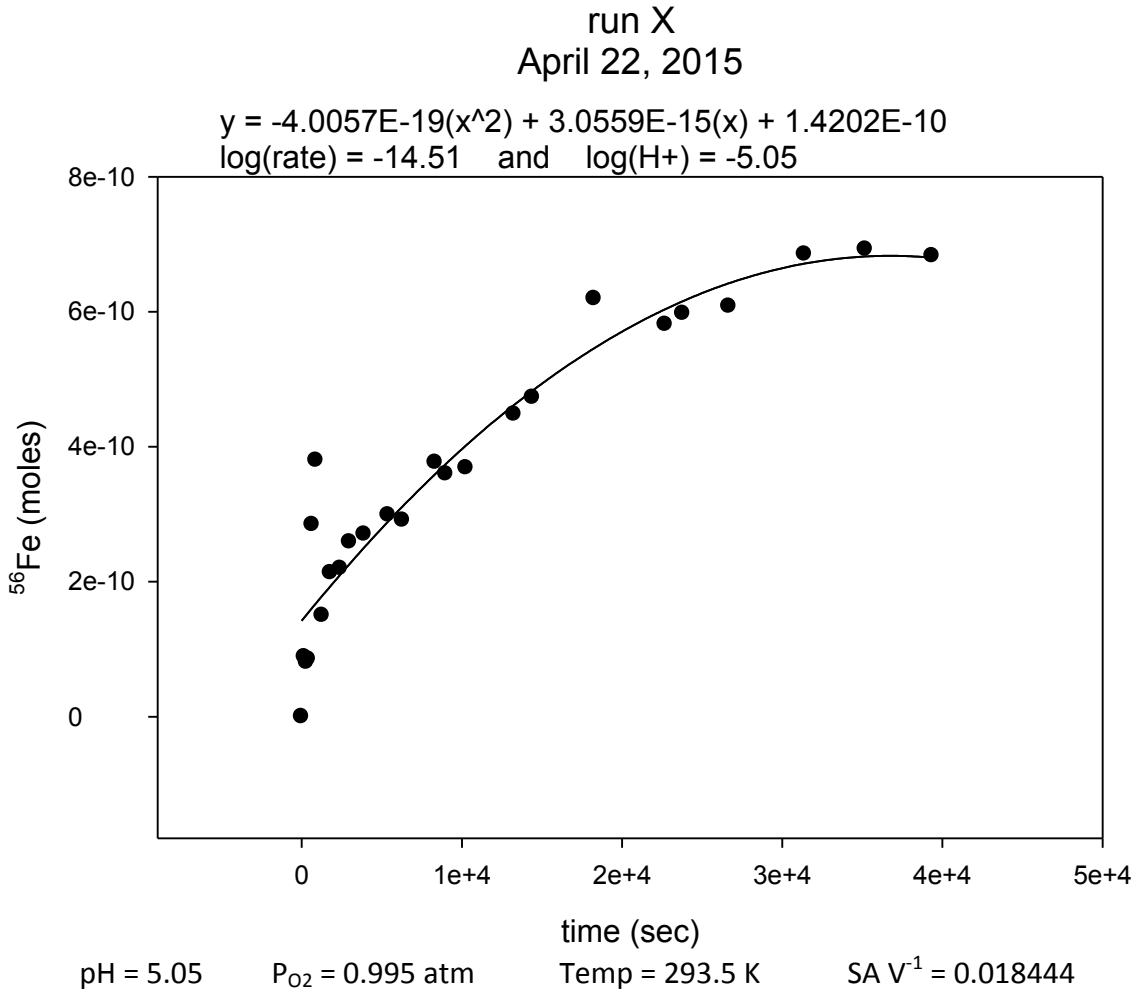
run X
April 22, 2015
y = -4.0057E-19(x^2) + 3.0559E-15(x) + 1.4202E-10
log(rate) = -14.51 and log(H+) = -5.05
8e-10
6e-10
4e-10
2e-10
0
56Fe (moles)
0
1e+4
2e+4
3e+4
4e+4
5e+4
time (sec)
pH = 5.05
P$_{O2}$ = 0.995 atm
Temp = 293.5 K
SA V^{-1} = 0.018444

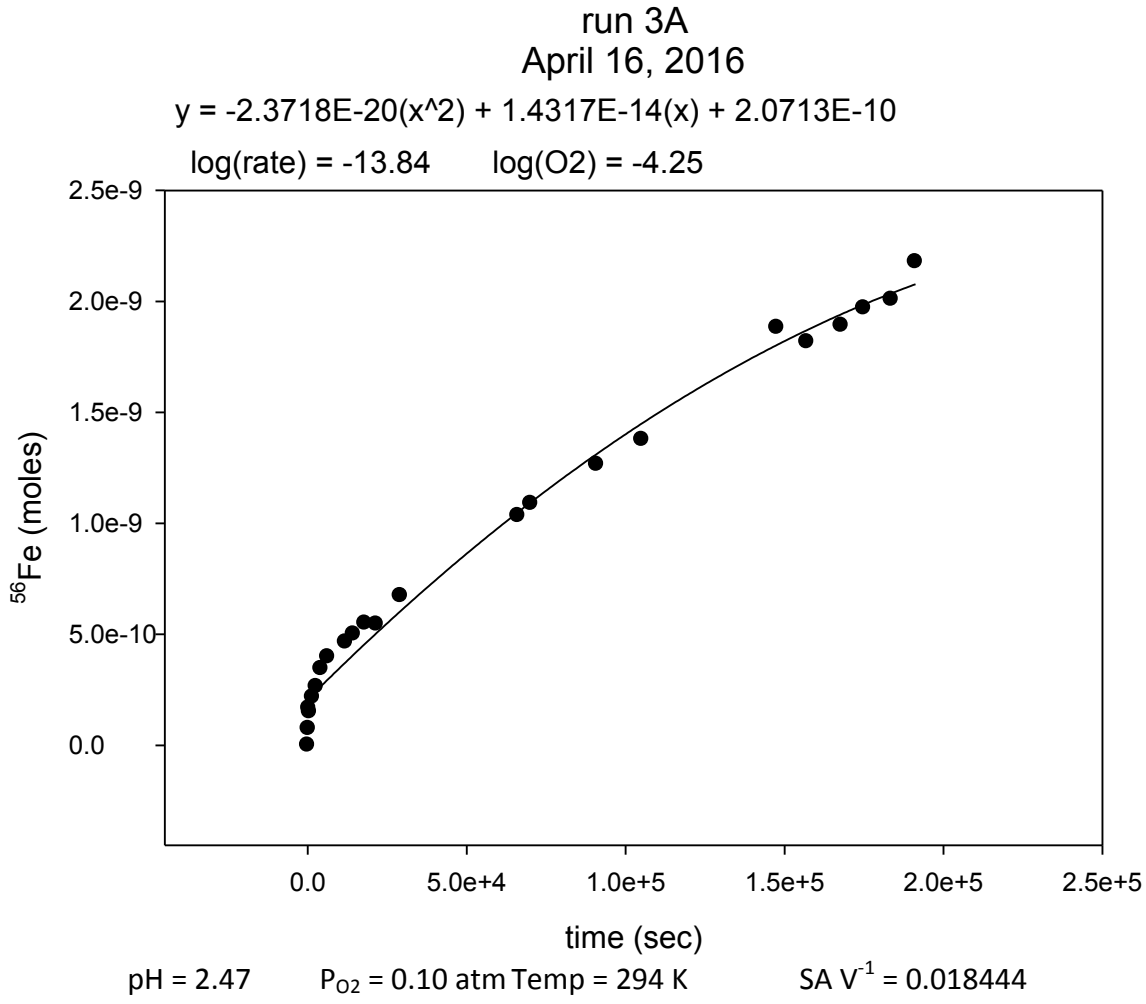
run 3A
April 16, 2016
y = -2.3718E-20(x^2) + 1.4317E-14(x) + 2.0713E-10
log(rate) = -13.84 log(O2) = -4.25
2.5e-9
2.0e-9
1.5e-9
1.0e-9
5.0e-10
0.0
56Fe (moles)
0.0
5.0e+4
1.0e+5
1.5e+5
2.0e+5
2.5e+5
time (sec)
pH = 2.47 PO2 = 0.10 atm Temp = 294 K SA V-1 = 0.018444

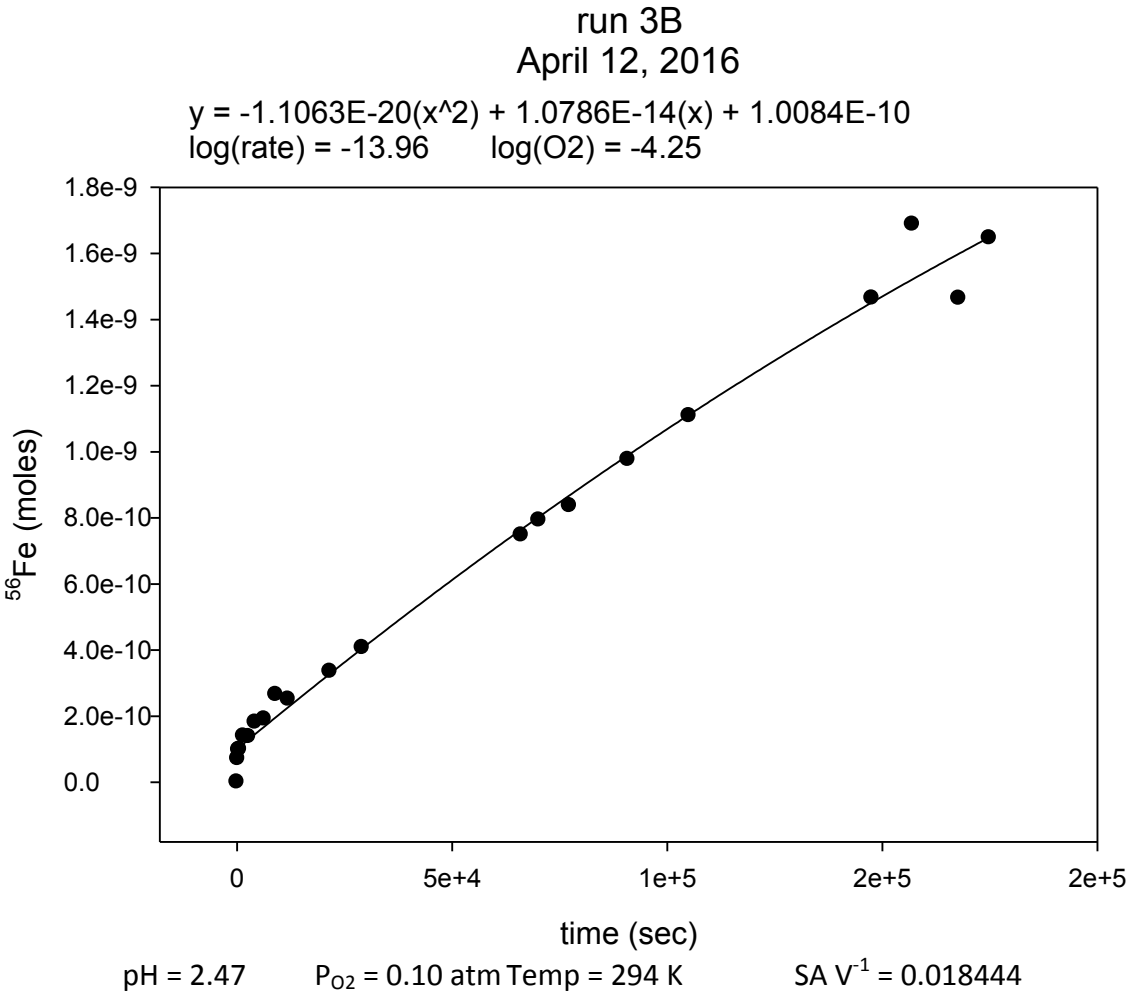
run 3B
April 12, 2016
y = -1.1063E-20(x^2) + 1.0786E-14(x) + 1.0084E-10
log(rate) = -13.96 log(O2) = -4.25
1.8e-9
1.6e-9
1.4e-9
1.2e-9
1.0e-9
8.0e-10
6.0e-10
4.0e-10
2.0e-10
0.0
56Fe (moles)
0
5e+4
1e+5
2e+5
2e+5
time (sec)
pH = 2.47
PO2 = 0.10 atm
Temp = 294 K
SA V-1 = 0.018444

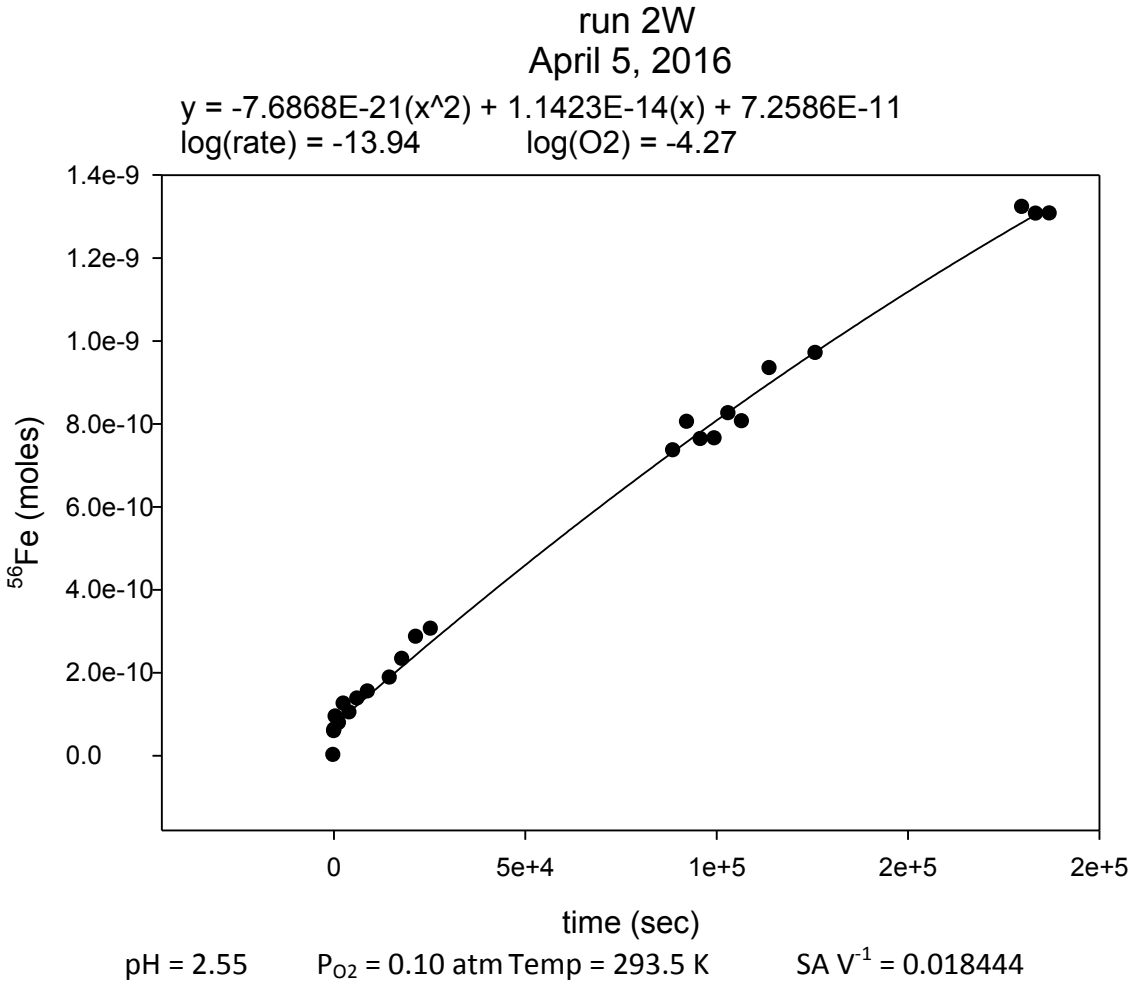
run 2W
April 5, 2016
y = -7.6868E-21(x^2) + 1.1423E-14(x) + 7.2586E-11
log(rate) = -13.94
log(O2) = -4.27
1.4e-9
1.2e-9
1.0e-9
8.0e-10
6.0e-10
4.0e-10
2.0e-10
0.0
56Fe (moles)
0
5e+4
1e+5
2e+5
2e+5
time (sec)
pH = 2.55
PO2 = 0.10 atm
Temp = 293.5 K
SA V-1 = 0.018444

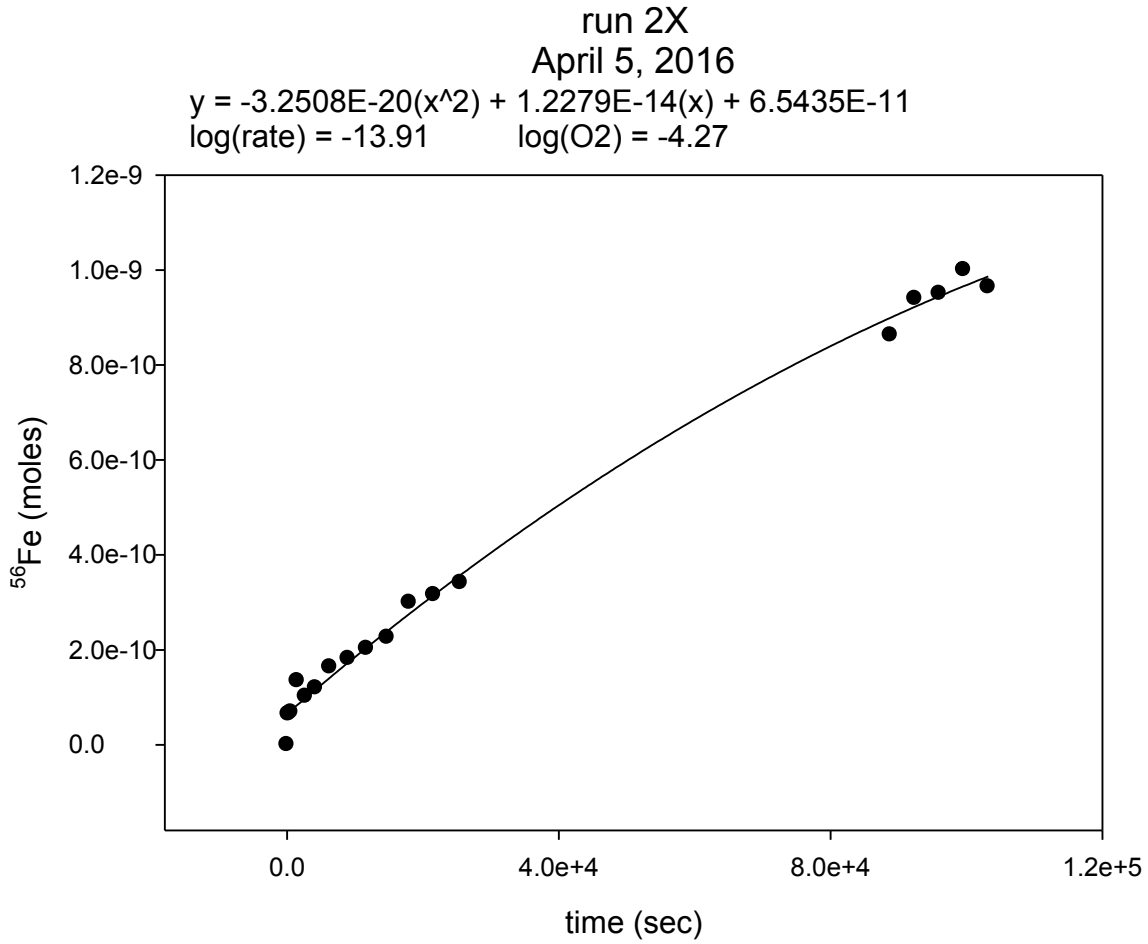

pH = 2.55 P_{O2} = 0.10 atm Temp = 294 K SA V^{-1} = 0.018444

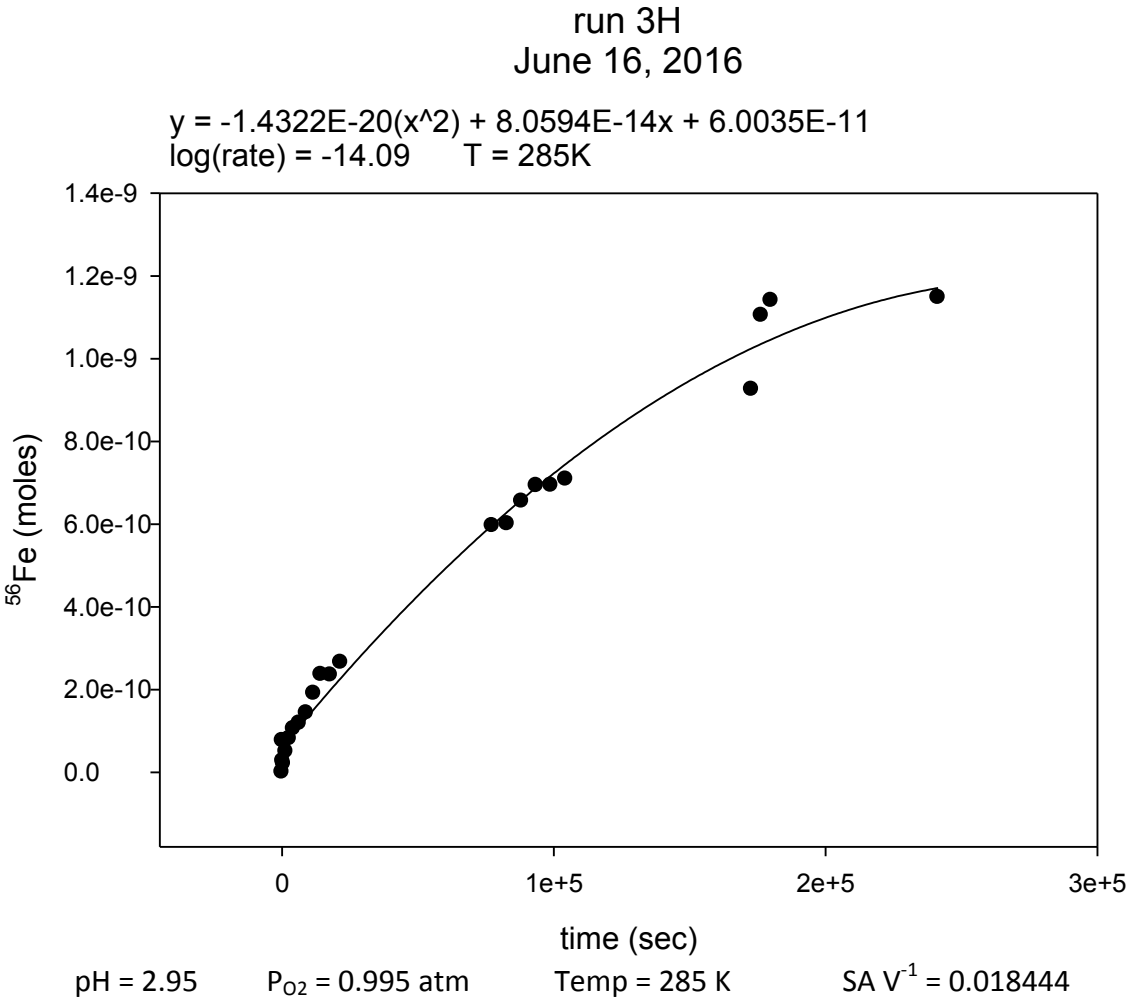
run 3H
June 16, 2016
y = -1.4322E-20(x^2) + 8.0594E-14x + 6.0035E-11
log(rate) = -14.09 T = 285K
1.4e-9
1.2e-9
1.0e-9
8.0e-10
6.0e-10
4.0e-10
2.0e-10
0.0
56Fe (moles)
0
1e+5
2e+5
3e+5
time (sec)
pH = 2.95
PO2 = 0.995 atm
Temp = 285 K
SA V-1 = 0.018444

run 3l
June 17, 2016

y = -3.3804E-20(x^2) + 5.479E-14x + 5.0271E-11
log(rate) = -13.26 T = 303K

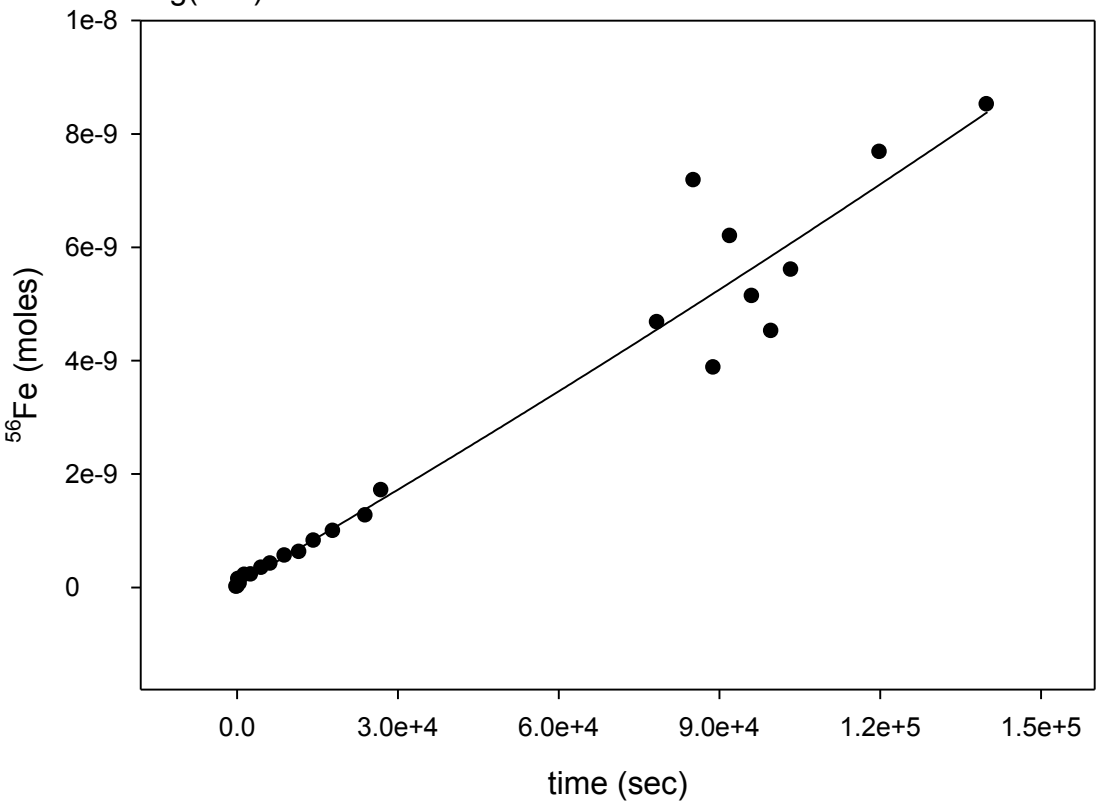

pH = 2.98 P_{O2} = 0.995 atm Temp = 303 K SA V^{-1} = 0.018444